ELSEVIER

Contents lists available at ScienceDirect

Desalination

journal homepage: www.elsevier.com/locate/desal



Membrane crystallization for recovery of lithium carbonate crystals: Study on process parameters and salts effect for Li₂CO₃-NaCl-KCl-LiCl solutions

Mohammad Mahdi A. Shirazi^a, Aamer Ali^b, Cejna Anna Quist-Jensen^{a,*}

- a Center for Membrane Technology. Department of Chemistry and Bioscience. Aalborg University. Fredrik Baiers Vei 7H, 9220 Aalborg East. Denmark
- b Department of Energy, Aalborg University, Pontoppidanstræde 111, 9220 Aalborg East, Denmark

HIGHLIGHTS

- Li₂CO₃ crystals were recovered by membrane crystallization.
- Feed temperature dominates the Li2CO3 crystal formation.
- NaCl and KCl delay the formation of crystals.

ARTICLE INFO

Keywords: Lithium carbonate (Li₂CO₃) Lithium recovery Membrane crystallization (MCr) Inorganic salts Solubility Ionic strength

ABSTRACT

In this work, membrane crystallization (MCr) process was employed for recovery of lithium carbonate (Li₂CO₃) crystals from synthetic brine solutions. First, the effect of the main operating conditions in MCr, including feed temperature (40, 50, and 60 °C) and flowrate (0.81, 1, and 1.3 L/min) was investigated on the crystallization of Li₂CO₃ in a binary solution. Next, the effect of main inorganic salts in the brine solutions (i.e., NaCl, KCl, and LiCl) and the mixture of them on the MCr performance and crystallization of Li₂CO₃ were investigated. In-line microscope, light microscope, scanning electron microscope, and X-ray diffraction test were used to observe the crystallization and characterize the obtained crystals. The obtained results revealed that feed temperature is the main parameter to dominate the nucleation and crystal formation and growth. Thus, the higher the feed temperature, the faster the crystal formation and the larger the crystals. The average crystal size increased from 9.59 to 30.51 μ m, when the feed temperature increased from 40 to 60 °C, respectively. However, smaller crystals were observed with adding NaCl and KCl to the solution. Moreover, none of the operating parameters nor the salts additives did affect the crystals shape and the obtained Li₂CO₃ crystals possess needle-like shape.

1. Introduction

Massive amount of minerals is available in the high salinity liquid resources, also known as brine, such as geothermal water, reject stream in the seawater desalination (RO brine), salt lakes, and produced water from oil and gas exploration [1,2]. These sources contain considerable amount of various metallic and non-metallic elements [3,4]. Among the available minerals in the brine resources, however, lithium (Li) has recently received enormous interest. For example, during the last two decades, the demand for Li has increased almost 10 folds. This has led to about 300 % increase in the Li price, just during the years 2020 to 2021 [5]. All these are due to exponential rising demand of Li in various industrial sectors [6,7]. The main Li consumer is the lithium-batteries

industry for electronic devices and heavy-duty vehicles [6]. It is predicted that an exponential growth up to 4.5 million tons per year by 2100 will be expected for the Li market to support these fast-growing sectors in the modern industry [8]. Among various available Li salts (e.g., LiCl, LiOH, LiHCO₃, etc.), lithium carbonate (Li₂CO₃) is highly demanded in the commercial scale due to its wide applications in commercial products, such Li-ion batteries, pharmaceutical products, etc. [9,10].

Lithium salt production includes three main steps, i.e., pretreatment and inorganic impurities removal, brine concentration and Li extraction. Various techniques have been introduced to pretreat and concentrate Licontain brine resources. For example, in the solar evaporation ponds, brine is pumped to a series of large evaporation ponds, and they undergo

E-mail address: cejna@bio.aau.dk (C.A. Quist-Jensen).

^{*} Corresponding author.

months-long sun evaporation1. After removing competing ions and other impurities, and reaching appropriate concentration in the evaporation ponds, LiCl-rich solution is delivered to a recovery plant [11]. Chemical precipitation, solvent extraction, and electrochemical techniques have also been investigated for the Li extraction step. For example, in chemical precipitation, materials such as Lime and sodium carbonate (Na₂CO₃) are added to the concentrated brine to remove Mg²⁺ and Ca²⁺ [12]. Another option includes electrochemical techniques which mainly realize the embedding and removal of Li in a proper electrode material by controlling the potential, so as to achieve the purpose of Li extraction from brine [13]. However, these techniques are suffered from major challenges such as low efficiency, chemicals contaminations, production and demand constraints, and environmental concerns [13–15]. Other modern approaches, such as membrane technology, therefore, could gain more attention due to numerous advantages, which have extensively been discussed in the literature [16–18]. Nanofiltration (NF), for example, is a chemical-free separation process, which can separate monovalent and divalent salts from brine and then concentrate it to make a Li-rich solution. However, it suffers from high operating pressure and low recovery value [19]. Forward osmosis can also enrich the brine up to relatively high concentrations. However, it cannot separate interfering salts and a proper and efficient draw solution as well as the membrane fouling are still challenging [20,21]. Other membrane tools, such as the supported liquid membrane and ion-sieve membranes, have also been investigated to run the separation processes for Li extraction. However, they are still far from the industrialization step due to expensive materials for membrane fabrication and scaleup issues [1,22,23]. Membrane crystallization, however, is an interesting and emerging technology, which can combine the separation and concentration steps into one, and simultaneously recover minerals and produce highly pure water, which can be quite interesting for further Li recovery and other industrial applications [24,25].

Membrane crystallization (MCr) is a non-isothermal separation process which offers numerous advantages over pressure-driven membrane processes and traditional precipitation. For example, MCr possesses less fouling/scaling tendency, needs very low operating pressure, can process feed streams with high concentration of solutes, and is almost a chemical-free recovery process. The high quality permeate stream generated by MCr can be further used in various industrial applications [26,27]. Moreover, one of the distinguishing features of MCr in comparison to conventional crystallization methods is in its ability to separate the nucleation process from the crystal growth process [28]. In particular, the rate of nucleation on the membrane surface can be one to two orders of magnitude greater than that of the bulk due to the elevated supersaturation on the membrane surface in contrast to the relatively lower level seen in the bulk [29]. All these have made MCr as an interesting and promising unit operation for recovery of a wide range of materials and minerals, such as phosphorous (P) [30] and inorganic ions (e.g., Na, K, Ag, Mg, B, etc.) in form of minerals [31–36]. MCr has also been investigated for Li-brine enrichment, however, it is still quite new to Li recovery from brine and efforts were focused on using MCr for removing inorganic impurities from the brine and producing a LiCl-rich solution [37-39]. Despite all these advantages and efforts, the implementation of this technology on a commercial scale has not been completely realized. The primary challenges in this way include energy efficiency, membrane material and its longevity, sustained performance over extended periods, and crystal quality, all towards efficient scale-up methodologies. There are some extensive studies for dealing with these issues, as MCr and MD are very similar in principles [40-42]. However, the crystal quality and effects of MCr parameters and impurity presence in MCr for Li₂CO₃ recovery purpose has remained an issue. It is important to acknowledge that previously mentioned conventional methods used for pretreating brine to eliminate competing ions are not anticipated to exhibit ideal selectivity towards the passage of Li. This is particularly true when considering the initial high concentration of other monovalent ions. Consequently, it is expected that the feed stream

of MCr will contain a significant presence of these other ions as well. This phenomenon can occur within a significant range for some salts, including NaCl, KCl, etc. [43].

In this work, the effect of major operating parameters including feed temperature and flowrate, on MCr performance as well as the crystallization of $\rm Li_2CO_3$ crystals was investigated, experimentally. Moreover, the effect of impurities including individual salts (NaCl, KCl, and LiCl) and their mixture in the brine solution on MCr performance and $\rm Li_2CO_3$ crystallization was explored. The objectives of this work include:

- Investigating the application of the MCr process for crystallization of Li₂CO₃ under various operating conditions
- Investigating the effect of brine composition on the crystallization of Li₂CO₃.

The quality of crystals is a crucial determinant of the economic viability of MCr systems, given that the sales of these crystals contribute significantly to the overall income. Results of this work could potentially provide valuable insights into the optimization of the MCr process for high quality Li₂CO₃ crystals recovery.

2. Materials and methods

2.1. Feed solutions

To run the experiments, 3 L of the feed solution was produced by dissolving lithium carbonate (Li₂CO₃) (7.5 g/L) in distilled water. Sodium chloride (NaCl) (5.8, 17.5, and 29.2 g/L), potassium chloride (KCl) (0.5, 1.5, and 2.5 g/L), and lithium chloride (LiCl) (2.11 g/L) were used as additives in the brine solution with various concentrations similar and close to the real RO brine solutions [44]. Moreover, a brine solution with mix of salts (containing 5.8 g/L of NaCl, 0.5 g/L of KCl, and 2.11 g/L of LiCl) was also used for MCr experiments. The concentration of Li₂CO₃ was considered high enough to shorten the membrane distillation part and enable the system to recover enough crystals for sampling and analyzing. All chemical reagents were used without further purification.

2.2. MCr setup and process

A lab-made hollow fiber module made of 21 capillary polypropylene (PP) membranes (0.2 μm pore size, 1.8 mm inner diameter, 450 μm thickness, 73 % porosity; MEMBRANA), was used for the experiments. Hollow fiber module design can provide the maximum packing density and effective surface area in comparison with other module designs, making them a favorable module design in industry and commerce [45], and thus, the obtained results from the lab-scale experiments can be used for scaling-up studies. Therefore, in this work, we used the hollow fiber module design for MCr experiments.

Fig. 1 shows the general scheme of the lab-scale MCr setup. Five thermocouples were used for monitoring temperature, four for the inlet and outlet temperatures of the feed and permeate channels, and one for monitoring the temperature of the feed/crystallization tank. Heating (Grant) and cooling (Julabo 200F) systems were used to maintain the temperature of the feed and permeate streams, respectively. A peristaltic pump (1.7 to 2900 mL/min; Masterflex L/S) was used for recirculation of the hot and cold streams under the same flowrates.

For the first set of experiments, three different feed temperatures (i. e., 40, 50, and 60 \pm 1 °C) under constant flowrate, and three different flowrates (i.e., 0.81, 1, and 1.3 L/min; corresponding to linear velocities of 0.069, 0.085, and 0.111 m/s, respectively) under constant feed temperature, were investigated. The permeate weight was measured using a digital balance (A&D, FZ-3000i; d = 0.01 g) during the tests. After each run, the membrane system was well washed through recirculation of cold and hot deionized water, respectively, each run for 1 h. The permeate flux of the membrane module was also measured using distilled water before and after experiments, to check the effect of

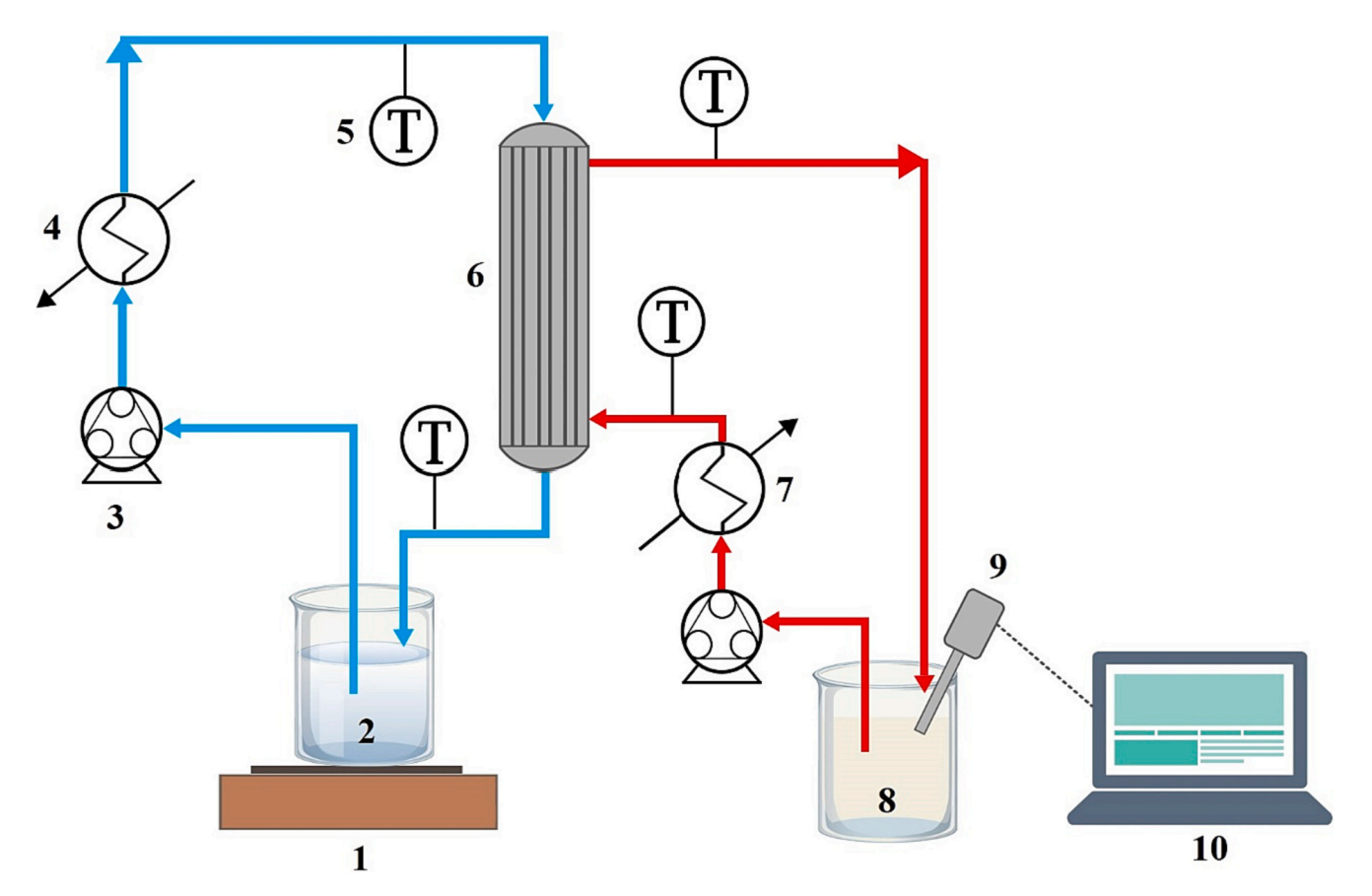


Fig. 1. A general scheme of the lab-scale MCr system (1: balance, 2: permeate tank, 3: peristaltic pump, 4: cooler, 5: thermocouple, 6: hollo fiber module, 7: heater, 8: feed/crystallization tank, 9: inline microscope, and 10: computer for data collection).

possible scaling on the membrane surface.

The permeate flux in the MCr process can be expressed as follows [46]:

$$J = \frac{\Delta m}{A \times t} \tag{1}$$

where Δm , A, and t are the collected permeate mass (kg), membrane surface (m²), and the interval time (h), respectively. The water recovery factor for the brine solution can be defined as follows:

$$RF(\%) = \frac{V_{removed}}{V_{initial}} \times 100 \tag{2}$$

where RF, $V_{removed}$, and $V_{initial}$ are the water recovery factor, the removed permeate volume from the feed tank, and the initial volume of the feed tank, respectively. The logarithmic average temperature difference along the membrane module can also be calculated as follow:

$$log T_{ln} = \frac{\left(T_{fi} - T_{po}\right) - \left(T_{fo} - T_{pi}\right)}{ln\frac{\left(T_{fi} - T_{po}\right)}{\left(T_{fo} - T_{pi}\right)}}$$
(3)

In this equation, T_{fi} and T_{fo} represent the inlet and outlet temperatures of the feed stream, while T_{pi} , and T_{po} represent the inlet and outlet temperatures of the permeate stream, respectively [47].

Moreover, it should be noted that a crystal recovery system nor a prefiltration step before the membrane module were not used in the experimental system, as the main objective of this research was the investigation of MCr performance and presence of inorganic impurities on the crystallization of Li_2CO_3 during the membrane crystallization process.

2.3. Crystal analysis

During the MCr experiments, an inline microscope (ParticleView V19, METER TOLEDO) was utilized for the purpose of observing the crystal formation during the crystallization. An external optical light microscope (a Zeiss Axiolab 5 fitted with an Axiocam 208 color) was also utilized to analyze the obtained crystals. For the purpose of sampling, about 1 mL of the crystal-containing solution was taken from the mother liquid and placed in a separate container. After spreading the sample out on the glass plate, images were captured of the crystals. During the analysis of the crystal images, an open-source program, i.e., ImageJ, was used. Scanning electron microscopy (SEM) (EVO, Zeiss) was also used to provide a clear image of the obtained crystals and their morphology.

In each of the experiments, X-ray diffraction (XRD) analysis was performed using a PANalytical Empyrean equipped with a Cu kappa alpha emitter in order to examine the structure of the crystals. Details of the procedures for crystals analysis can be found in the previous works [2,31,48]. Moreover, the crystal elongation (L/W) is defined by the ratio of length (L) to width (W) of crystals. The elongation ratio indicates the conversion in the crystal shape from a needle to a rectangular, and vice versa.

To analyze the effect of operating parameters and salts presence on MCr performance, and crystals formation, the results at same range of water recovery (RF = 60 %) were investigated and compared.

3. Results and discussion

3.1. Effect of operating parameters

3.1.1. Effect of temperature

Fig. 2 illustrates the experimental results (i.e., permeate flux,

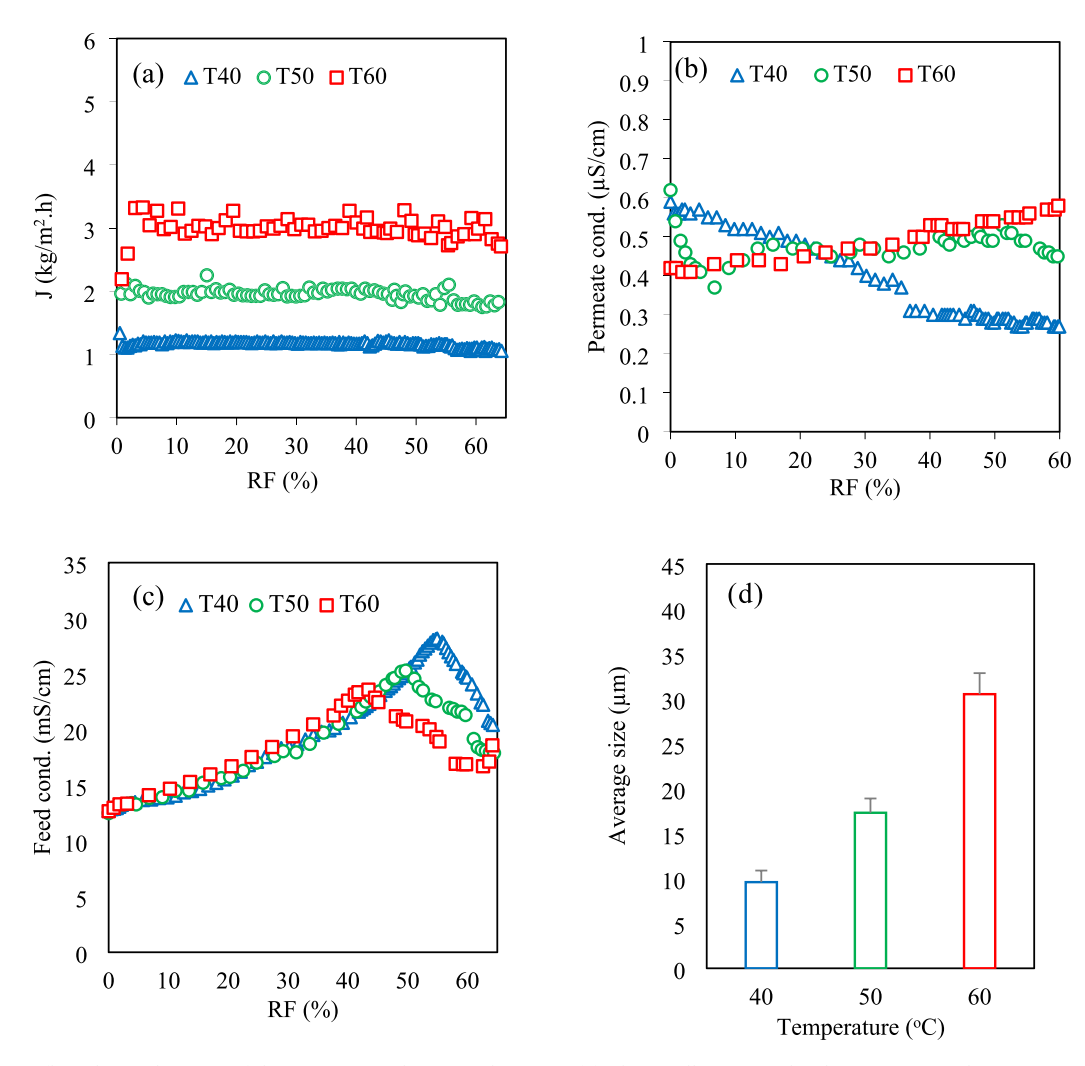


Fig. 2. (a) Permeate flux, (b) conductivity of the permeate tank, (c) conductivity of feed/crystallization tank, (d) average crystal size, (e) crystals elongation, (f) coefficient of variation, and (g) XRD patterns for the obtained crystals, for MCr experiments at different feed temperatures (40, 50, and 60 ± 1 °C) and constant flowrate (1.3 L/min).

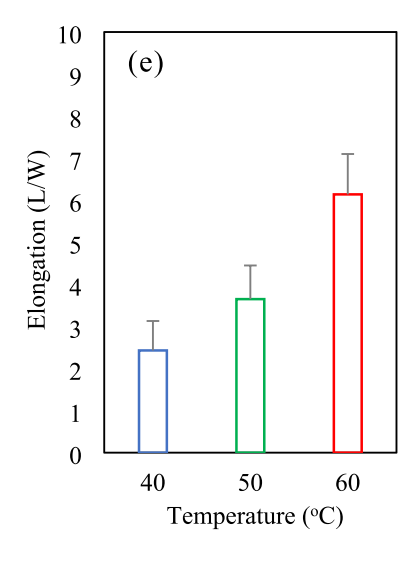
conductivity of the permeate tank, conductivity of the feed/crystallization tank, all versus water recovery, as well as average crystal size, crystal elongation, coefficient of variation, and XRD patterns) at different feed temperatures (40, 50, and 60 \pm 1 $^{\circ}$ C). Fig. 3 also shows the SEM crystal images at different feed temperatures.

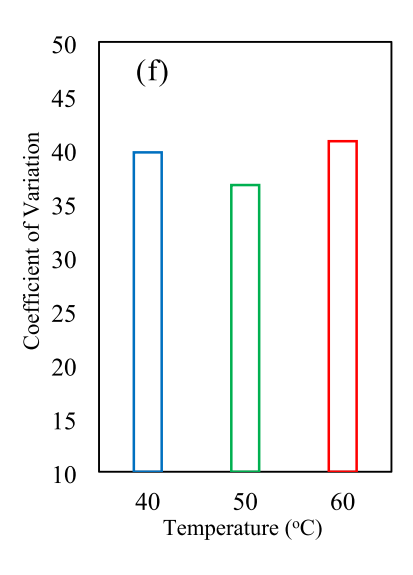
As could be observed (Fig. 2-a), higher permeate flux was provided when the feed temperature increased from 40 to 60 °C. For example, the initial permeate fluxes were measured at 1.33, 1.96, and 3.32 kg/m²·h for the feed temperatures of 40, 50, and 60 \pm 1 °C, respectively. The average fluxes before starting the crystallization were also measured at about 1.18, 1.98, and 3.01 kg/m²·h for the investigated feed temperatures (40-60 °C), respectively. This is in good agreement with the reported results in the literature regarding the effect of feed temperature on the permeate flux [49–51]. The higher permeate flux at higher feed temperatures attributes to higher vapor pressure difference, which is the driving force in MD. Thus, the higher the feed temperature, the higher the driving force, and consequently the higher the permeate flux [52]. The permeate flux, however, gradually, and slightly decreased after starting the crystallization although the logarithmic average temperature difference (Eq. (3)) remained almost constant (Fig. S1-a). This can be attributed to the higher solute concentration on the membrane surface, also known as the concentration polarization [53]. Moreover, the permeate flux was more stable at the lowest feed temperature (40 °C),

while it slightly fluctuated for the highest feed temperature (60 \pm 1 $^{\circ}$ C). This can also be attributed to ease of temperature control at low temperature ranges, while it can fluctuate at higher ranges.

Due to the formation of crystals and variation in the salt content of the feed stream, the overall trend for changing in the conductivity of the permeate tank is reported as the indicator of the permeate quality. Fig. 2-b provides the change in the conductivity of the permeate tank, during the MCr experiments at different feed temperatures. As could be observed, the conductivity of the permeate tank slightly changed for all experiments. However, it remained lower than 1 μ S/cm, even after a long test with low feed temperature (40 °C) for >24 h. This indicates that the MCr system with PP membranes could perform properly for crystallization of Li₂CO₃ solutions at different feed temperatures. This is also in good agreement with the reported results in the literature indicating the high solute rejection in MD and MCr processes, even if a highly saline brine is introduced to the system [28,42,54].

Fig. 2-c shows the changes in the conductivity of the feed/crystallization tank versus water recovery factor (Eq. (2)) at different feed temperatures (40, 50, and 60 °C), while flowrate was kept constant. As could be observed, the conductivity of the feed solution increased with increasing the solute concentration, and then decreased with starting the crystallization. However, the change in the trend of the conductivity of the feed solution happened at different water recovery factors. The





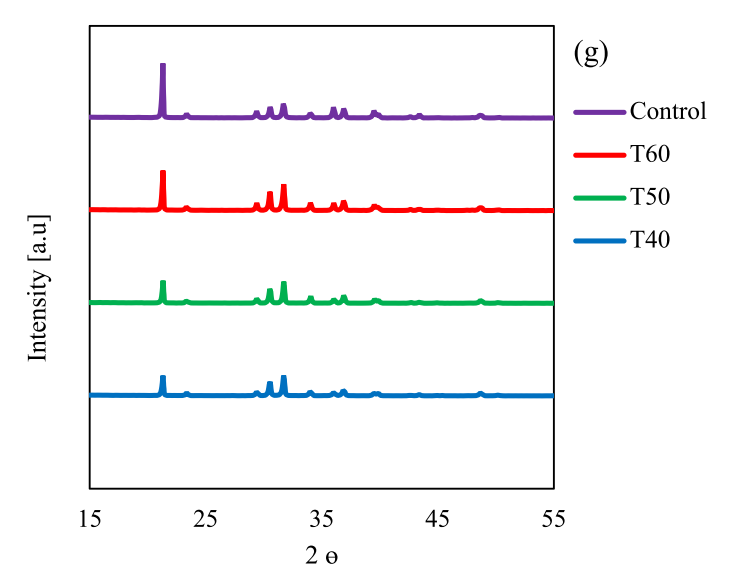


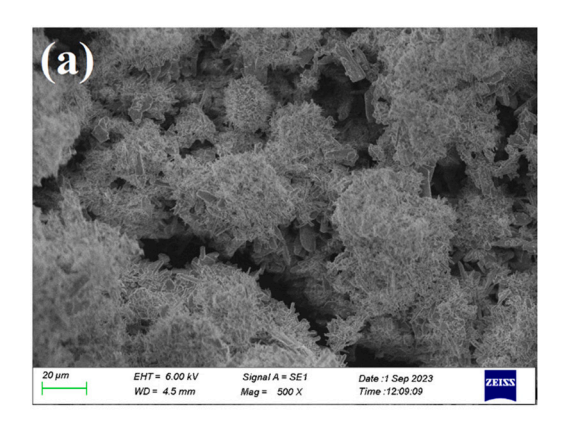
Fig. 2. (continued).

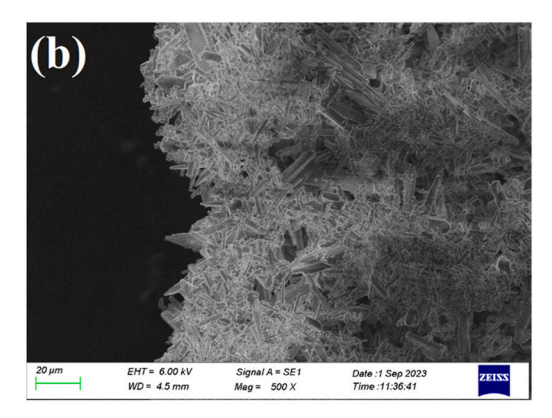
corresponding water recovery factor for starting the crystallization was measured at 50.5, 47.8, and 41.7 % for feed temperatures of 40, 50, and 60 °C, respectively. This can be attributed to the effect of temperature on the solubility of Li₂CO₃ in water (Fig. S3-a). Although Li₂CO₃ is not highly water soluble like other lithium salts, such as LiCl, its solubility can slightly change with temperature. The solubility of Li₂CO₃ was reported at 11.45, 10.78, and 9.92 g/L at 40, 50, and 60 °C, respectively [55]. However, the corresponding concentrations of Li₂CO₃ when the crystallization started were calculated at different values, i.e., 15.17, 14.37, and 12.87 g/L, at feed temperatures of 40, 50, and 60 °C, respectively. This can be explained by induction time and the required supersaturation for starting the nucleation. Further explanation is provided in the caption of Fig. S5.

Fig. 2-d and -e show the average crystal size and the crystals elongation at various feed temperatures. The crystal elongation is defined as the length to width ratio. This parameter indicates the transformation of the crystals shape from a rectangular to a needle-like one, and vice versa. As could be observed, the average crystal size increased with increasing the feed temperature (Fig. 2-d). For example, the average size for crystals at temperature 40 was calculated at \sim 9.6 μ m and it increased up to \sim 30.5 μ m at feed temperature of 60 °C. The same trend could be observed for crystal elongation (L/W) (Fig. 2-e), however, with smaller

change, when L/W ratio increased from 2.4 to 6.1 for the feed temperature increment from 40 to 60 °C, respectively. According to these results, it can be argued that the $\rm Li_2CO_3$ crystals mainly grow in length rather than in width, providing a needle-like shape when the feed temperature is increased (Fig. 3). Moreover, larger average crystal size at higher feed temperature can be attributed to both the higher permeate flux (Fig. 2-a) and lower solubility of the solute (Fig. S2-a). Both of these issues can provide faster supersaturation and therefore, faster crystal growth, which could provide larger crystal sizes with elongated shape. While the coefficient of variation (CV) of crystals for the experiments at different temperatures is in the range of 36–40 (Fig. 2-f), it decreased from 40 to 50 °C, and then increased for experiment at 60 °C.

Furthermore, the crystallinity and phase purity of the obtained crystals from different experiments as well as a commercial $\rm Li_2CO_3$ sample (the top graph as the control), were measured using the XRD test (Fig. 2-g). Lithium carbonate is a monoclinic crystal and the XRD peaks can be appeared at 21.40° , 23.50° , 29.53° , 30.60° , 31.84° , 34.20° , 36.17° , and 37.08° . These peaks are corresponding to (110), (200), (111), (-202), (002), (-112), (020), and (-311) crystal planes, respectively [56]. As could be observed, all the peaks for obtained crystals at different feed temperatures are well-matched with commercial $\rm Li_2CO_3$ sample. Therefore, it can be concluded that the operating





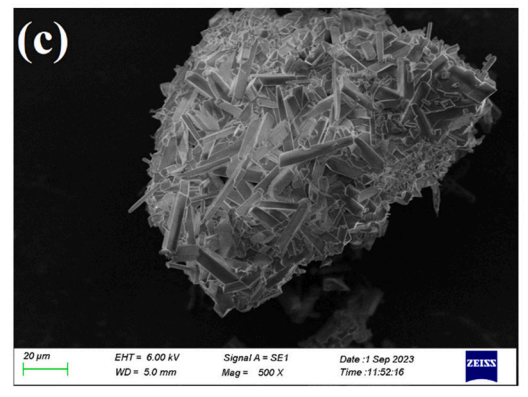


Fig. 3. SEM images of Li₂CO₃ crystals at different feed temperatures of (a) 40, (b) 50, and (c) 60 °C, at the constant flowrate of 1.3 L/min, all at the same water recovery (60 %).

temperature did not affect the quality of the obtained crystals.

Fig. 3 shows the SEM images of the obtained crystals at different temperatures of 40, 50, and 60 $^{\circ}$ C, all at the same RF value of 60 %. As could be observed from the appearance, larger crystals were achieved with increasing the feed temperature, and this is quite well along with the crystal size measurement results (Fig. 2-d). This goes back to the effect of feed temperature on the solubility of the Li₂CO₃, as it was discussed above. The images of the Li₂CO₃ crystals obtained from light microscope are also presented in Fig. S2.

3.1.2. Effect of flowrate

Fig. 4 presents the experimental results (i.e., permeate flux, conductivity of the permeate tank, conductivity of the feed/crystallization tank, all versus water recovery, as well as average crystal size, crystal elongation, coefficient of variation, and XRD patterns) at different flowrates (0.81, 1, and 1.3 L/min), when the feed temperature was kept constant at $60 \pm 1~^{\circ}\text{C}$.

As could be observed, almost similar permeate flux was measured for experiments at different flowrates, while the feed temperature was kept constant at 60 \pm 1 $^{\circ}$ C. The average permeate flux before starting the crystallization was measured at ~3 kg/m²·h for all experiments at different flowrates (0.81, 1, and 1.3 L/min). Comparing Figs. 2-a and 4-a revealed that the feed temperature was more effective in terms of the permeate flux in MCr process. This can be attributed to the effect of the operating parameters on the driving force of MCr process. As the MCr is a non-isothermal separation, the driving force (i.e., vapor pressure difference across the membrane pores) is more affected by the average temperature difference along the membrane module (Eq. (3)), than the flowrate. This is in good agreement with the literature on the effect of flowrate and feed temperature on the permeate flux [57,58]. Moreover, the conductivity of the permeate tank remained $<1~\mu\text{S/cm}$ for all experiments. Although, a very slight change with increasing trend could be observed with the experiment at highest flowrate (1.3 L/min), it can be

argued that the permeate was not contaminated with the solute in the permeate stream. This is evidence shows that pore wetting did not occur, even after starting the crystallization step (Fig. 4-b).

Fig. 4-c shows the variation in the conductivity of the feed/crystal-lization tank during the experiments at different flowrates. As could be observed, the conductivity of the feed solution changed when the crystallization started. However, unlike the experiments at different temperatures (Fig. 2-c), the flowrate did not affect the crystallization starting point significantly. The water recovery factor of the crystallization point was calculated at 44.8, 42.4, and 41.7 % for flowrates of 0.81, 1, and 1.3 L/min, respectively. This can be explained as follow.

The above observation can be explained based on the solubility change in proportion of feed temperature [59]. In case of Li₂CO₃, the solubility decreases with increasing the temperature (Fig. S3-a). Thus, it can be expected that the crystallization happens at almost similar RF for all experiments at different flowrates when the feed temperature was kept constant (60 \pm 1 $^{\circ}$ C). The slight difference in RF value of the crystallization point can also be attributed to the lower temperature drop in the feed tank before the crystallization is started due to faster recirculation of the feed solution. As could be seen in Fig. S4, the higher the flowrate, the higher the feed tank temperature, when the feed temperature is kept constant (60 \pm 1 $^{\circ}$ C). However, after starting and proceeding the crystallization, higher temperature drop in the feed/ crystallization tank could be observed. Moreover, higher flowrate could provide faster transfer of solute molecules to the crystal lattice at higher flowrate as well as the possibility of secondary nucleation due to the excessive cross flow velocity [60] (i.e., 0.81, 1, and 1.3 L/min; corresponding to linear velocities of 0.069, 0.085, and 0.111 m/s, respectively). However, these effects can be marginal in comparison with the influence of feed temperature on crystallization. Furthermore, the higher flowrate can also reduce the effect of crystals accumulation and deposition inside the tubes and the vertical membrane module at higher water recovery factors, when considerable amount of crystal is

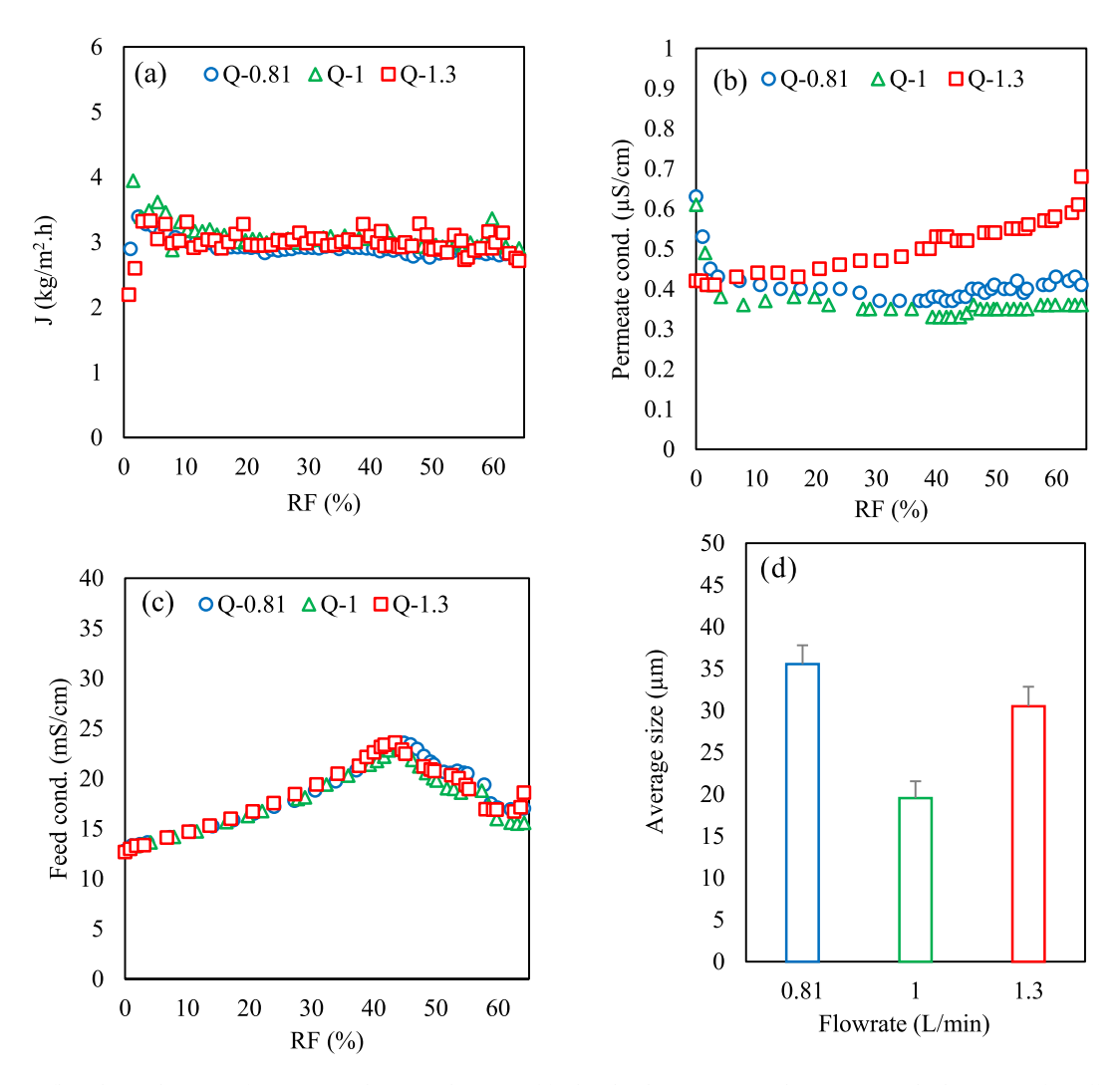


Fig. 4. (a) Permeate flux, (b) conductivity of permeate tank, (c) conductivity of feed tank, (d) average crystal size, (e) crystals elongation, (f) coefficient of variation, and (g) XRD patterns of obtained crystals, for MCr experiments at different flowrates (0.81, 1, and 1.3 L/min) and constant feed temperature (60 \pm 1 $^{\circ}$ C).

presented and circulated in the system, as observed during our experiments. While it is quite necessary for experiments at high RF (RF > 70%), no crystal recovery system was used in this work for the MCr setup.

The average crystal size for experiments at different flowrates is shown in Fig. 4-d. The largest value was measured for the lowest flowrate. With increasing the flowrate from 0.81 to 1 L/min, the average crystal size decreased from \sim 35 to \sim 19 µm, and then increased again up to ${\sim}30~\mu m$ for the highest flowrate. The effect of flowrate on the crystal growth and the crystal size is proportional to a limiting step. This limiting step can either be the ion diffusion into the crystal lattice or the nuclease attachment on to the crystal lattice. Considering this, the higher flowrate can facilitate the ion transport to the crystal lattice and provide faster crystal formation. However, lower flowrate can impose less shear and stress to the formed crystals, and consequently fewer collision among the crystals is expected. Therefore, while faster crystal formation (i.e., crystal formation at lower water recovery) can be expected with increasing the flowrate, the average crystal size may not follow a specific trend due to the crystals breakage and deformation when they possess needle-like shape. Therefore, this fluctuation in the average crystal size can be expected for needle-like Li₂CO₃ crystals (Fig. S4) at various flowrates, as the crystals breakage does not follow a uniform pattern. However, it can be concluded that the higher flowrate is beneficial for reducing the effect of crystal deposition on the membrane surface and its accumulation in the system during the experiments. This can be more beneficial if a crystal recovery step is also considered in the experimental system. Moreover, comparing the results of the average crystal size at different temperatures (Fig. 2-d) with the same parameter at different flowrate (Fig. 4-d), it can be concluded that the feed temperature can be consider as a dominant parameter affecting the crystals size.

Fig. 4-e shows the elongation of crystals at different flowrate values. As could be observed, the overall trend of elongation values is similar to the average crystal size, i.e., it first decreased from 5.45 to 4.62 when the flowrate increased from 0.81 to 1 L/min, and then increased up to 6.14 when the flowrate increased up to 1.3 L/min. This indicates that higher flowrate could produce more needle-like crystals. Moreover, it also indicates that the feed temperature was more effective than that of the flowrate on the crystals shape and their elongation ratio. In terms of CV, the trend is different, i.e., it first increased and then decreased with increasing the flowrate. Comparing the changes in values of Figs. 2-f and 4-f can also provide another evidence for higher effect of feed temperature on the obtained crystals compared to the flowrate. However, these results are not in agreement with some arguments in the literature. For example, Chen et al. [61] investigated the effect of feed temperatures (60, 65, and 68 °C) and flowrates (0.35, 0.7, and 0.88 L/min) on the MCr response with a continuous mode for crystallization of RO brine. The authors reported that flowrate was more effective on MCr response in terms of the permeate flux and crystal size in comparison with feed

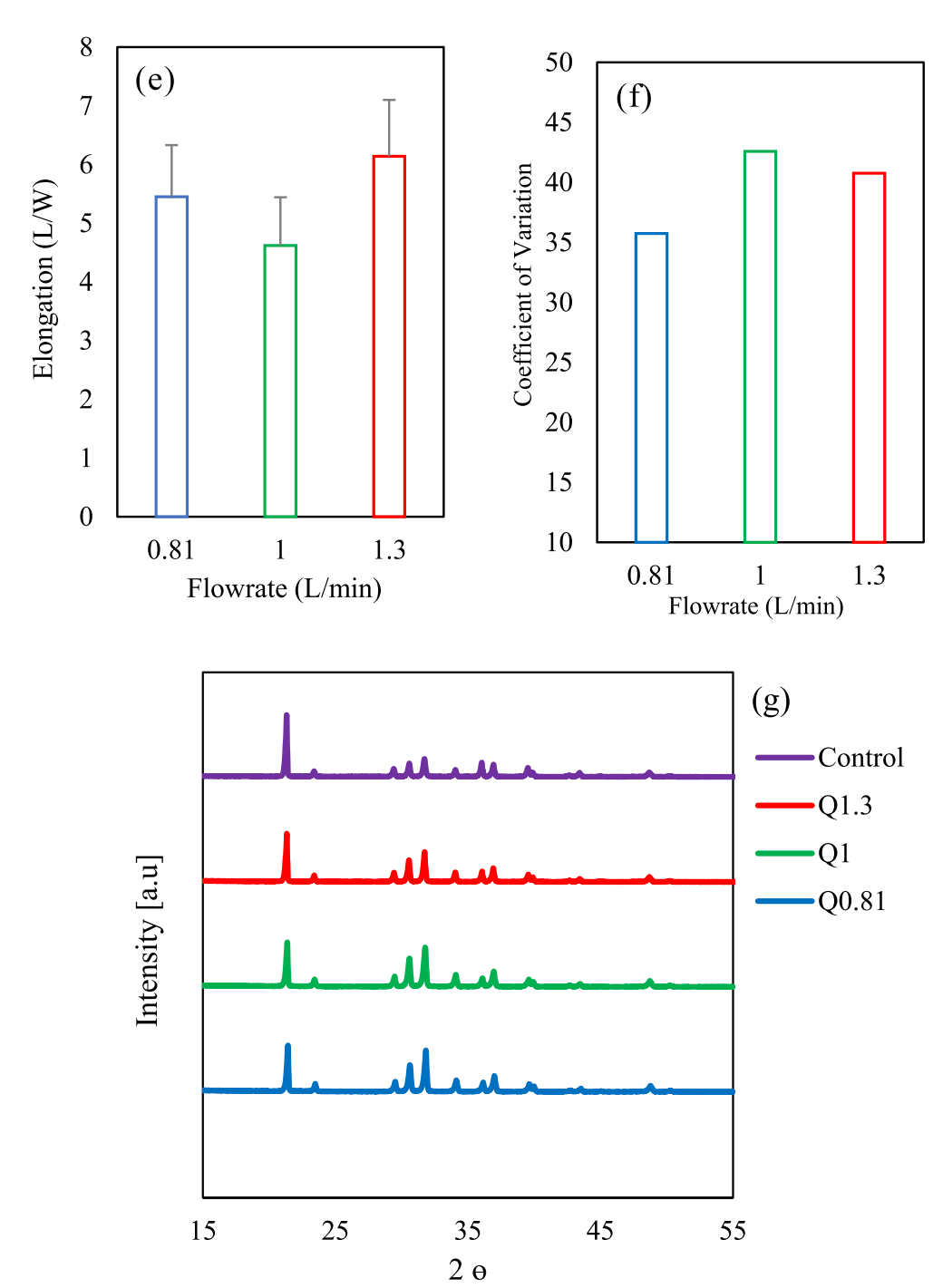


Fig. 4. (continued).

temperature. This difference between the Chen's results and the observed ones in this work can be attributed to the difference in the materials of crystals in these works, and the limited range of temperatures in the feed channel (ΔT_f : 8 °C [61]) compared to the range of flowrates. In another work, hasty flux decline and sharp increase in the conductivity of the permeate tank were reported [60]. It was argued that the sharp flux decline could be attributed to the formation of more scale on the membrane surface due to enhanced secondary nucleation at high flowrates. Scale formation and flux decline could also lead to increase in the permeate conductivity, maybe due to the partial pore wetting [60]. However, the increase in the flowrate did not considerably affect the permeate conductivity nor the crystals shape and elongation in this work (Fig. 4-b and -d).

Moreover, Fig. 4-g shows the XRD patterns for the obtained crystals from experiments at different flowrates. As could be observed, the obtained peaks are well-matched with the corresponding peaks of the commercial $\rm Li_2CO_3$, which was used as the control. Therefore, this can be argued that the flowrate did not affect the quality and crystallinity of obtained white powder from different experiments.

3.2. Effect of salt additives

3.2.1. NaCl presence

Fig. 5 shows the results of experiments for membrane distillation crystallization of Li_2CO_3 in the presence of sodium chloride (NaCl) at different initial concentrations (5.8, 17.5, and 29.2 g/L). In all figures,

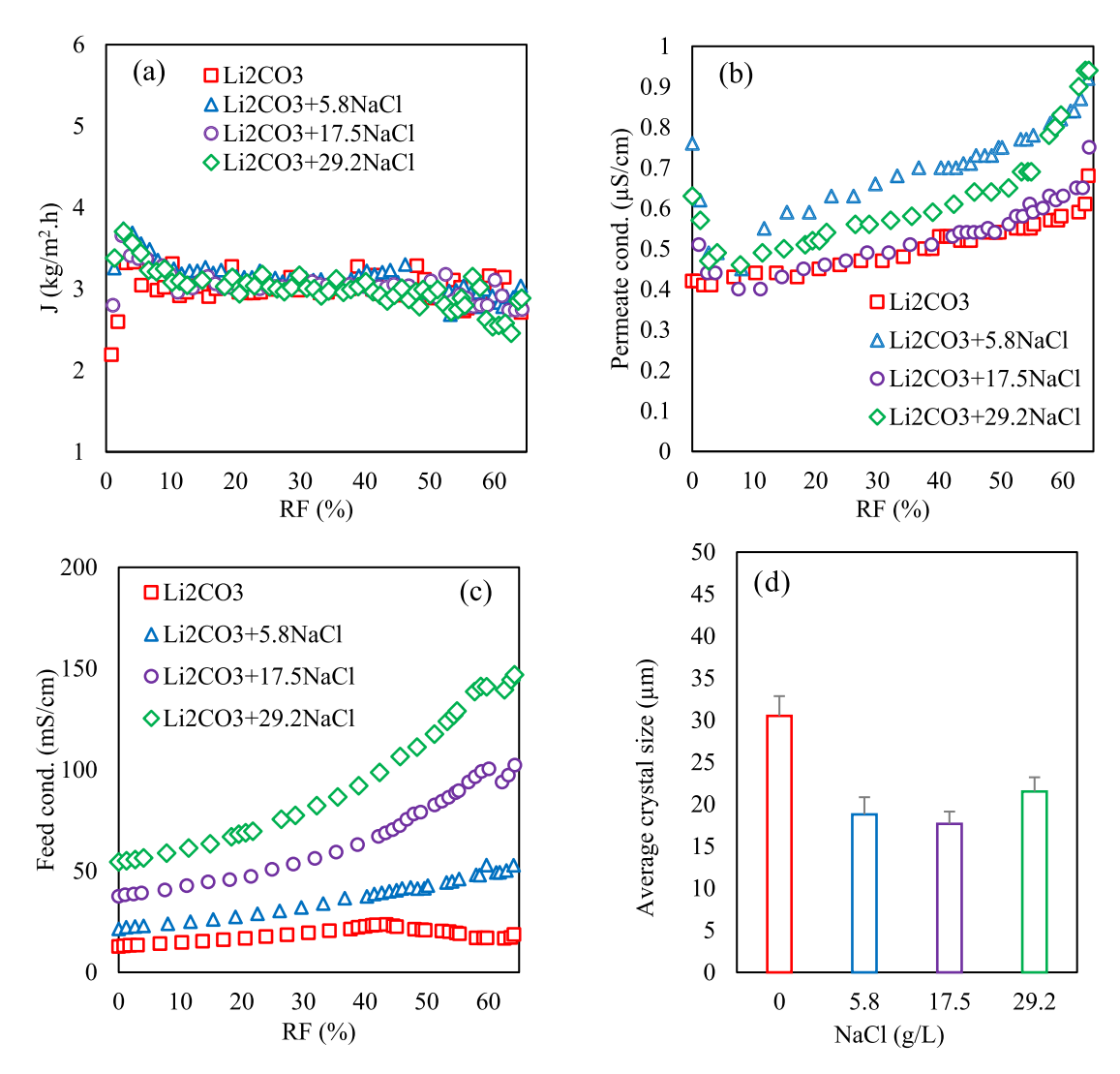


Fig. 5. (a) Permeate flux, (b) conductivity of permeate tank, (c) conductivity of feed tank, (d) average crystal size, (e) crystals elongation, (f) coefficient of variation, and (g) XRD patterns, for MCr experiments containing different NaCl concentrations (0, 5.8, 17.5, and 29.2 g/L) at constant feed temperature (60 \pm 1 $^{\circ}$ C) and flowrate (1.3 L/min).

the graph for the experiment at the same temperature with an NaCl-free solution of ${\rm Li_2CO_3}$ in pure water is also presented (in red) as the control for a better comparison. All experiments were carried out at constant operating conditions of 60 °C feed temperature and 1.3 L/min flowrate. Fig. 6 also shows the SEM images of the obtained crystals from various experiments.

Fig. 5-a presents the permeate flux versus water recovery for experiments at different initial concentrations of NaCl (0, 5.8, 17.5, and 29.2 g/L). The average permeate flux before starting the crystallization was measured at a same value of ~3 kg/m²·h, for different initial NaCl concentrations. It is worth quoting that the same membrane module was well-washed and used for experiments. Thus, it can be argued that the membrane fouling/scaling was negligible in the applied hollow fiber module. Obtaining a similar flux with different NaCl concentration in the feed solution is in good agreement with the fact that MCr is much less sensitive to the solute concentration in the feed stream in comparison with other membrane processes, such as pressure driven ones [62]. This is one of the advantages of MCr over other membrane technologies, which can process feed samples with high solute concentrations, such as high salinity brines [63]. Moreover, the produced water in the permeate tank possesses quite high purity, indicated by the conductivity of the permeate solution which remained below 1 µS/cm for all experiments,

regardless of the initial salt concentration (Fig. 5-b). For all the conducted experiments, however, the conductivity increased very slightly with increasing the water recovery. This can be explained as follows.

The pore wetting of the applied hydrophobic membrane is one of the most challenging obstacles of MCr [64]. The membrane wetting comprises three distinct steps: the unwetted step (in the absence of any partial penetration of the fed solution into pores), the transition step (some pores are partially penetrated), and the complete wetting step (some or all the pores are fully penetrated) [65]. When wetting occurs, the rapid penetration of liquid through the pores of the membrane often happens within a few seconds, leading to a fast change in the conductivity of the permeate tank [29]. As could be observed in Fig. 5-b, however, the conductivity of the feed tank remained very low (<1 μ S/cm). Therefore, the partial pore wetting can be neglected in this work.

Fig. 5-c shows the variation in the conductivity of the feed tank/crystallization for experiments at different initial NaCl concentrations in comparison with the control graph for the binary solution (Li_2CO_3 in pure water). As could be observed, unlike the NaCl-free feed stream, when NaCl is present in the solution, conductivity of the feed solution increases continuously even after starting the crystallization of Li_2CO_3 , as NaCl concentration is still far from the required supersaturation condition for its crystallization [66]. Moreover, the conductivity of the

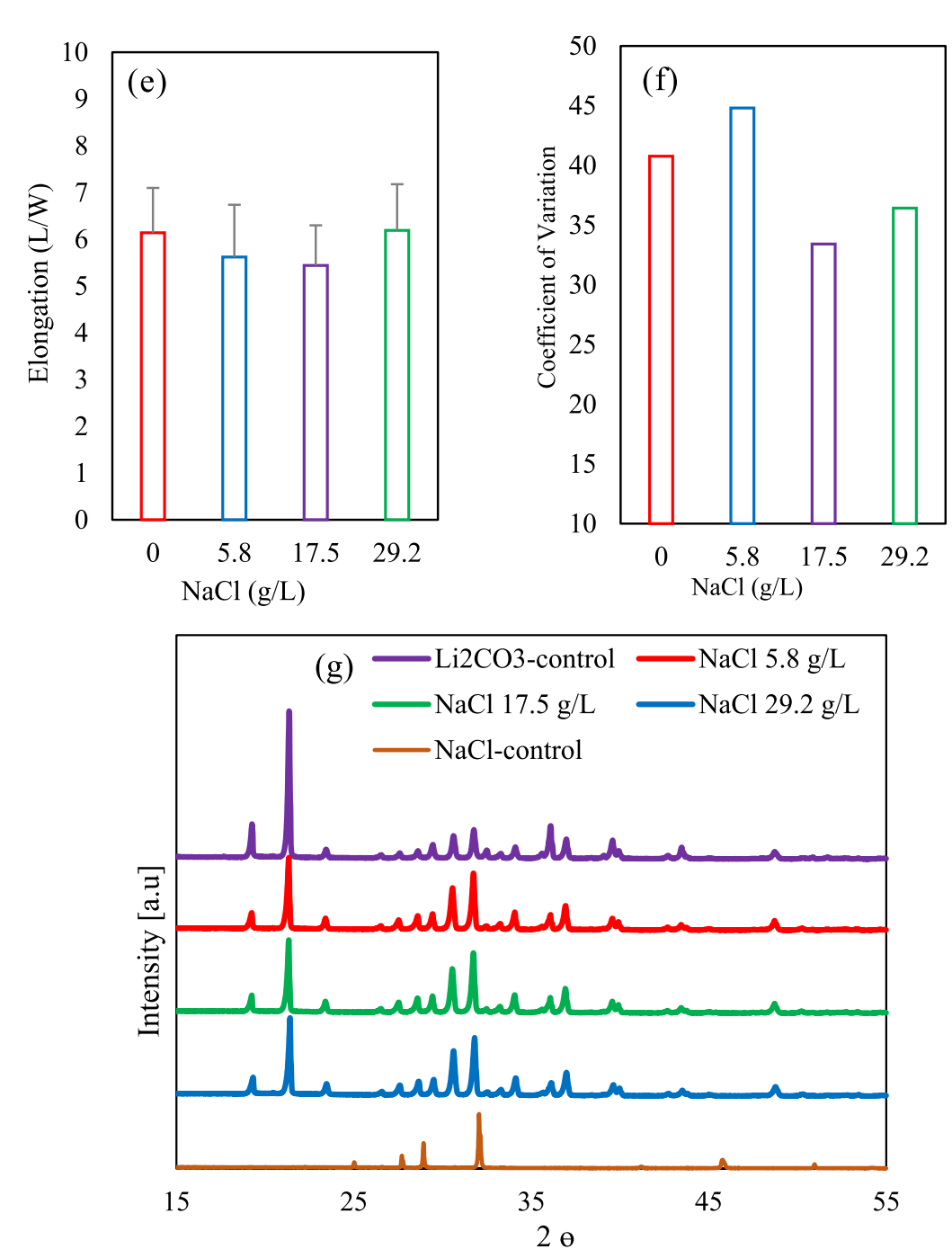
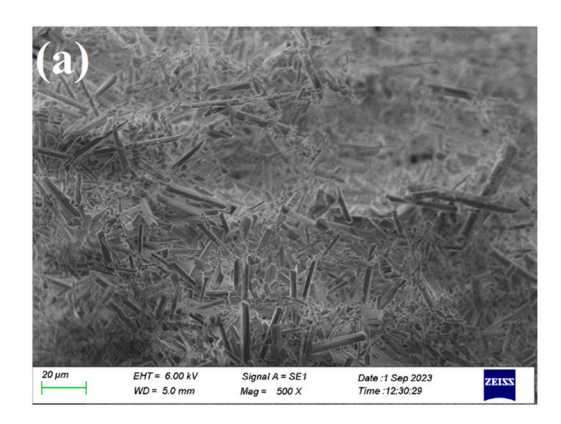


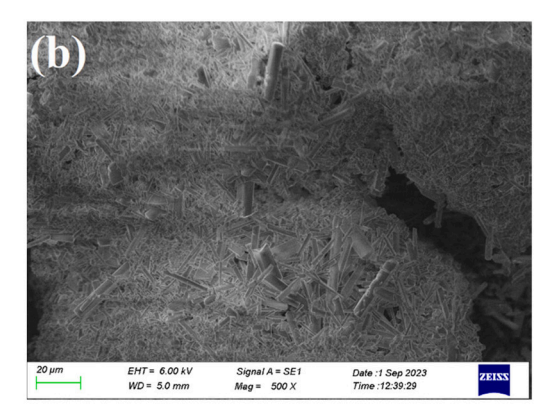
Fig. 5. (continued).

solution is affected not only by Li_2CO_3 , but also by NaCl. As a result, while Li_2CO_3 can precipitate, NaCl is remained dissolved in the solution and its concentration increases with increasing water recovery. This could therefore cause in increasing the overall conductivity of the feed solution. Moreover, although all experiments were conducted at the same operating conditions (60 °C and 1.3 L/min), the Li_2CO_3 crystals did not appear at the same water recovery factor. According to the obtained results, increasing in the initial concentration of NaCl could postpone the formation of Li_2CO_3 crystals. For example, the corresponding water recovery factors for experiments with initial NaCl concentration of 5.8, 17.5, and 29.2 g/L were measured at ~46, ~49, and ~48 %, respectively. This can be explained as follows.

The effect of adding inorganic salts into the ${\rm Li_2CO_3}$ solution can be explained according to common-ion effect or salting-out effect. The first

term describes the reduction in solubility of an ionic precipitate caused by the addition of a soluble molecule that shares an ion with the precipitate to the solution [67]. However, the solubility of a salt (such as Li_2CO_3 in this case) can occasionally be increased by introducing an ion other than those that are already present in the solution (such as NaCl in this case). This is known as the uncommon-ion effect, also known as the diverse-ion effect, which can cause salting-in phenomenon [68]. This can happen because inter-ion attraction within the solution can play a significant role when the total ion concentration rises [69]. Thus, the ions are less readily accessible for the crystallization process due to this alternative equilibrium. This is in good agreement with the literature indicating the effect of NaCl on the solubility of Li_2CO_3 in water. It is experimentally observed and proved that the addition of NaCl can increase the solubility of Li_2CO_3 at various temperatures (Fig. S6-a) [55].





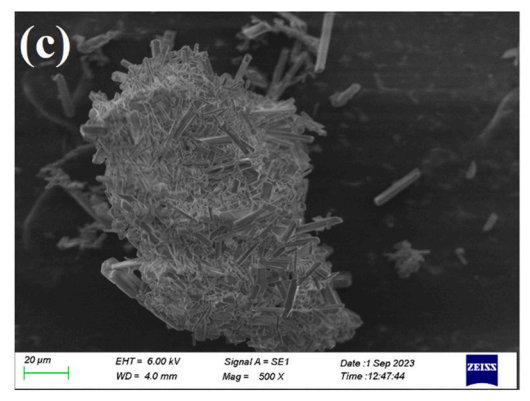


Fig. 6. SEM images of Li₂CO₃ crystals obtained from the feed solution with different NaCl content (5.8, 17.5, and 29.2 g/L), all at the same water recovery factor (60 %).

For this reason, the $\rm Li_2CO_3$ crystals appeared at higher water recovery with adding NaCl to the feed solution. These results can be useful for further development of MCr for $\rm Li_2CO_3$ recovery, either it is used for stepwise fractional brine processing or processing the NF-pretreated brine. In both cases, a complete removal of inorganic impurities cannot be achieved. For example, the maximum Na⁺ rejection of commercial NF membranes that are specifically developed for brine treatment was reported in the range of 20–30 % [44]. Higher removal (%) of inorganic impurities was reported in the literature using a fractional MCr process, while simple brine solutions have been considered [38]. However, these impurities, such as NaCl can remain in the brine, appear at high concentrations and affect the $\rm Li_2CO_3$ crystallization at high RF values (RF > 90 %).

The average crystal size of Li₂CO₃ is shown in Fig. 5-d. As could be observed, adding NaCl to the lithium solution led to decrease in the crystal size. For example, for the solution containing lithium carbonate and 5.8 g/L NaCl, the average crystal size decreased from ${\sim}30~\mu m$ to \sim 19 μ m, in comparison with the NaCl-free solution. Slightly more decrease in the average crystal size was observed with further increase in NaCl concentration up to 17.5 g/L. However, with more increase in the initial NaCl concentration the average crystal size increased slightly. These results are in good agreement with the effect of the presence of NaCl on the solubility of Li₂CO₃ [55]. Thus, it can be argued that the presence of NaCl showed a similar effect of lowering temperature. Moreover, this decrease in the crystal size in the presence of NaCl, which is considered as an impurity in the crystallization of Li₂CO₃, can also be attributed to the change in the nucleation interfaces. The presence of an impurity, such as an inorganic salt, can act as a supplemental nucleation site. With increasing the NaCl concentration, the available nucleation sites increase as well. Moreover, the presence of NaCl in the solution can provide Cl⁻ ion which can compete with CO_3^{2-} and increase the solubility of Li salt in the solution [55,70]. All these could then produce smaller crystals rather than bigger ones.

Although the similar trend was observed, the elongation ratio changed slightly with increasing the initial NaCl concentration in the feed solution. With comparison of Figs. 2-e and 5-e, it can be argued that the feed temperature increment showed more effect on the crystals' elongation. The CV was also calculated in the range of 30–45 (Fig. 5-f) for the obtained Li_2CO_3 crystals at different NaCl concentrations (Fig. 6).

Fig. 5-g shows the XRD patterns for the control samples (the top and bottom graphs show the pattern for the commercial ${\rm Li_2CO_3}$ and the commercial NaCl, respectively) and the obtained white powder samples from MCr experiments in the presence of different initial NaCl concentrations. As could be observed, the obtained patterns for the powders from the experiments are quite fit with the control pattern for ${\rm Li_2CO_3}$ and no peaks related to NaCl was observed. This could be expected and is in good agreement with the solubility trend of NaCl in water (Fig. S3-b). Fig. 6 also provides the SEM images of the obtained crystals from MCr experiments in the presence of NaCl with different initial concentrations. NaCl crystals possess a very defined cubic shape [63,71], and no cubic shape crystals which represent the presence of NaCl crystals were observed in any of the SEM images nor the microscopic images from various samples.

3.2.2. KCl presence

The results of MCr experiments for Li_2CO_3 solution in the presence of potassium chloride (KCl) at different initial concentrations (0.5, 1.5, and 2.5 g/L) are shown in Fig. 8. In all figures, the graph for the experiment at the same temperature with a binary solution of Li_2CO_3 in pure water is also presented (in red) as the control for a better comparison. All experiments were carried out at constant operating conditions of 60 °C feed temperature and 1.3 L/min flowrate. Fig. 9 also shows the images of the obtained crystals from various experiments.

As could be observed in Fig. 7-a, the trend for the permeate flux is almost the same for all experiments, including the MCr test with a binary $\rm Li_2CO_3$ solution and the same solution in the presence of KCl at different

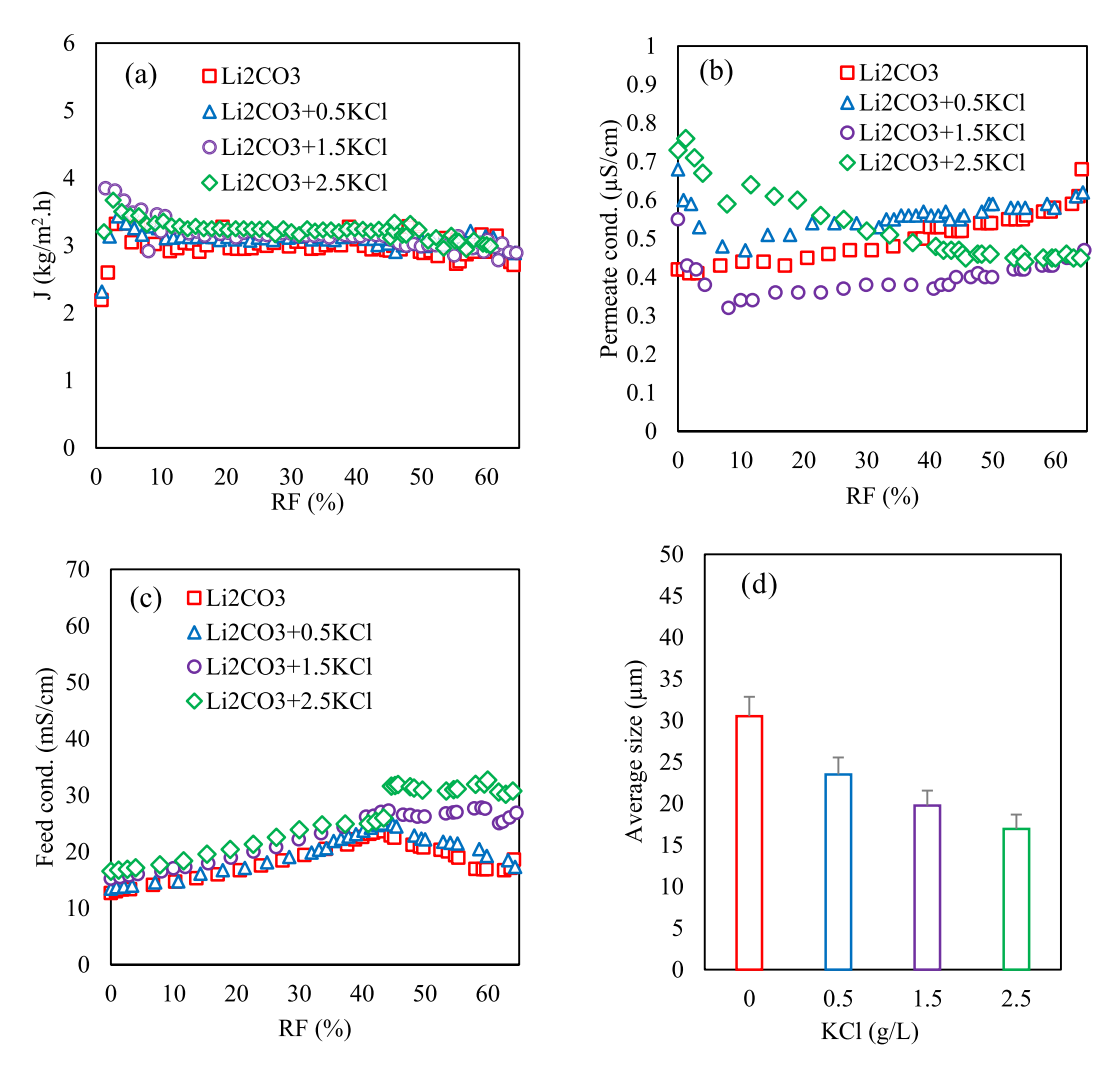


Fig. 7. (a) Permeate flux, (b) conductivity of permeate tank, (c) conductivity of feed tank, (d) average crystal size, (e) crystals elongation, (f) crystal size distribution, and (g) coefficient of variation, values for MCr experiments with different KCl concentrations (0, 0.5, 1.5, and 2.5 g/L) at constant feed temperature (60 ± 1 °C) and flowrate (1.3 L/min).

concentrations. The average permeate flux before starting crystallization for Li₂CO₃ solution and the feed sample containing KCl at different concentrations were measured at $\sim\!3$ kg/m $^2\cdot h.$ Moreover, the conductivity of the permeate tank remained below 1 $\mu S/cm$ (Fig. 7-b), which indicates a proper performance for MCr and the used hollow fiber PP membrane.

According to the obtained results, the crystals appeared at different water recovery factors with increasing in the KCl concentration in the solution. For example, for the binary solution of $\rm Li_2CO_3$ in water at 60 °C, the crystals appeared at water recovery of 41.7 %, while with increasing the KCl concentration in the solution from 0.5 to 2.5 g/L, the crystals appeared at 43.2, 44.1, and 45.7 %, respectively. This could make a change in the conductivity trend of the feed solution (Fig. 7-c), as well. This observation is in good agreement with the effect of adding KCl on the solubility of $\rm Li_2CO_3$ in water. In fact, the addition of KCl to a solution of lithium carbonate can increase the solubility of $\rm Li_2CO_3$ in water (Fig. S6-b) [55]. Similarly with the case of NaCl addition to the feed solution, this can also be attributed to the salting-in effect of KCl in the $\rm Li_2CO_3$ solution [72], which can affect the overall crystallization process via delaying the nucleation step [10].

As mentioned earlier, the salting-in effect of KCl addition to the $\rm Li_2CO_3$ solution can increase the solubility of the lithium salt in water. Thus, it can also affect the average crystal size as well. As could be

observed in Fig. 7-d, the average crystal size decreased with increasing the KCl concentration in the solution from 0 to 2.5 g/L. For example, in the absence of KCl, the average crystal size was calculated at $\sim\!30~\mu m$, while it decreased to $\sim\!17~\mu m$ when the initial concentration of KCl increased up to 2.5 g/L. Thus, this can be argued that the KCl addition to the feed solution possesses overall similar effect on the crystallization of Li_2CO_3 in the MCr process.

In terms of the crystals' elongation, although it decreased with adding KCl into the solution, however, it remained constant (i.e., $\sim\!4.5$) for all initial concentrations of KCl. Moreover, comparing Figs. 5-e and 7-e shows that KCl could affect the elongation of Li₂CO₃ crystals more than NaCl. The CV values were also calculated around 40 for the crystals obtained from the experiments at different KCl concentration, and with less fluctuation in comparison with CV values of crystals from Li₂CO₃ + NaCl solution. Moreover, Fig. 7-g provides the XRD patterns of the obtained powders from different MCr experiments of Li₂CO₃-KCl solutions. As could be observed, all peaks are well-fitted with the peaks of the control sample (commercial Li₂CO₃), indicating no precipitation of KCl in the crystallization step. This could also be expected as the solubility of KCl and other possible salts for the Li₂CO₃-KCl solution (e.g., K₂CO₃ and LiCl) are much higher than Li₂CO₃ [73].

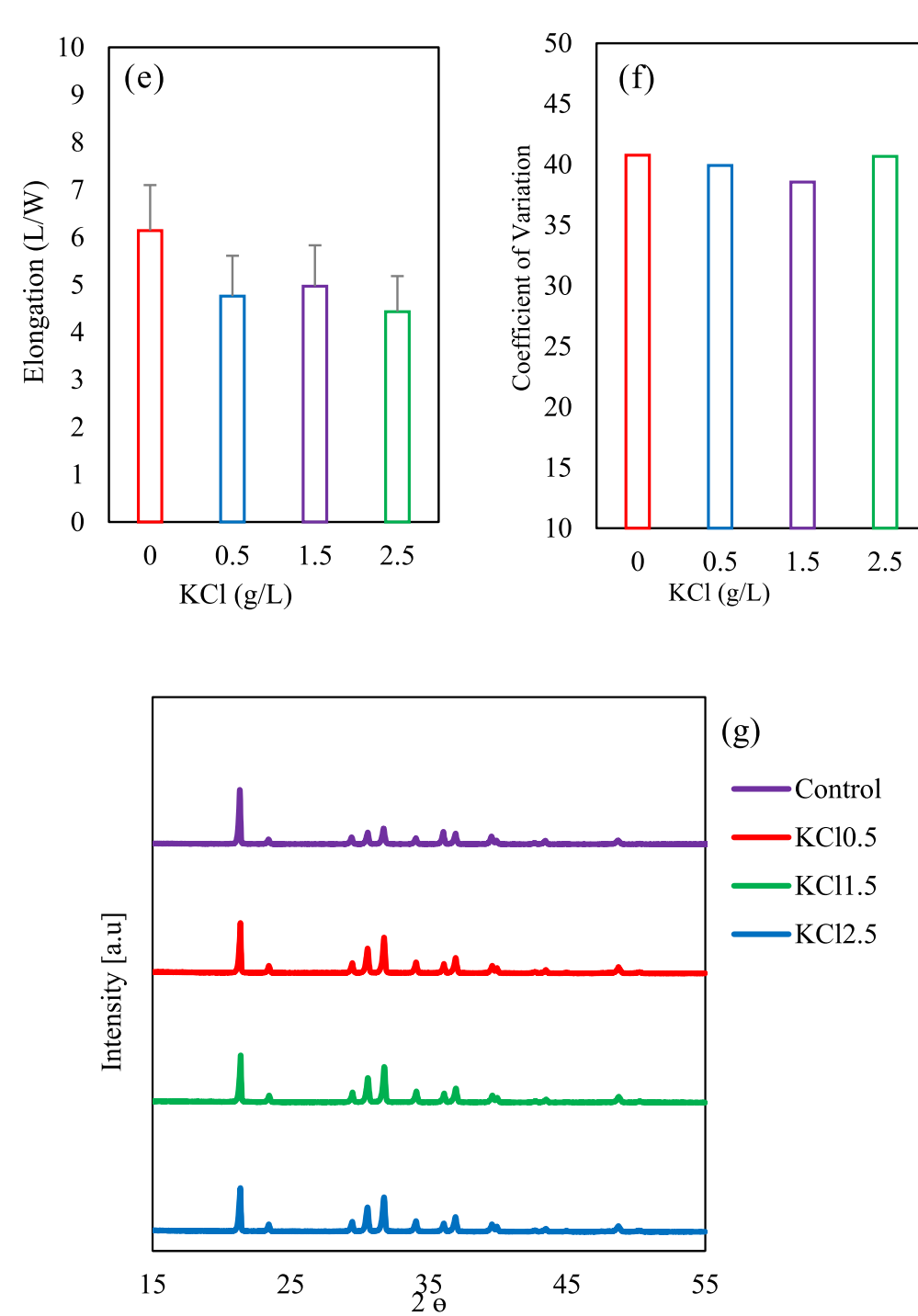


Fig. 7. (continued).

3.2.3. LiCl presence

Fig. 8 provides the results from the MCr experiment with adding LiCl (2.11 g/L) into the solution. This includes the MCr permeate flux, the conductivity of the permeate tank, the trend for conductivity of the feed/crystallization tank, crystal average size, crystal elongation, coefficient of variation, and XRD patterns. In this part, only one concentration was investigated for LiCl, as high concentration of LiCl would not be expected when LiCl-rich solution is converted to Li $_2$ CO $_3$ solution by adding proper chemicals, such as Na $_2$ CO $_3$ [11].

As could be observed, the trend in the permeate flux of MCr process and the conductivity of the permeate tank in the presence of LiCl in the feed solution is similar to other experiments. The average permeate flux before starting crystallization was measured at $\sim\!3\,\mbox{kg/m}^2\cdot\mbox{h}$, as the same

logarithmic average feed temperature could be achieved along the membrane module under the considered operating conditions (Fig. S1-e). However, the permeate flux slightly decrease after starting crystallization (Fig. 8-a). As discussed earlier, this can be attributed to the deposition of crystals on the membrane surface with increasing the water recovery factor. In terms of the permeate quality, the conductivity of the permeate tank again remained below 1 μ S/cm (Fig. 8-b), which indicates that the applied membrane could perform properly, and no pore wetting occurred. This high solute rejection can be expected for MCr in the absence of pore wetting [1].

Fig. 8-c shows that the conductivity of the feed/crystallization tank increased with increasing the water recovery from the feed solution. However, its trend changed after starting the crystallization and

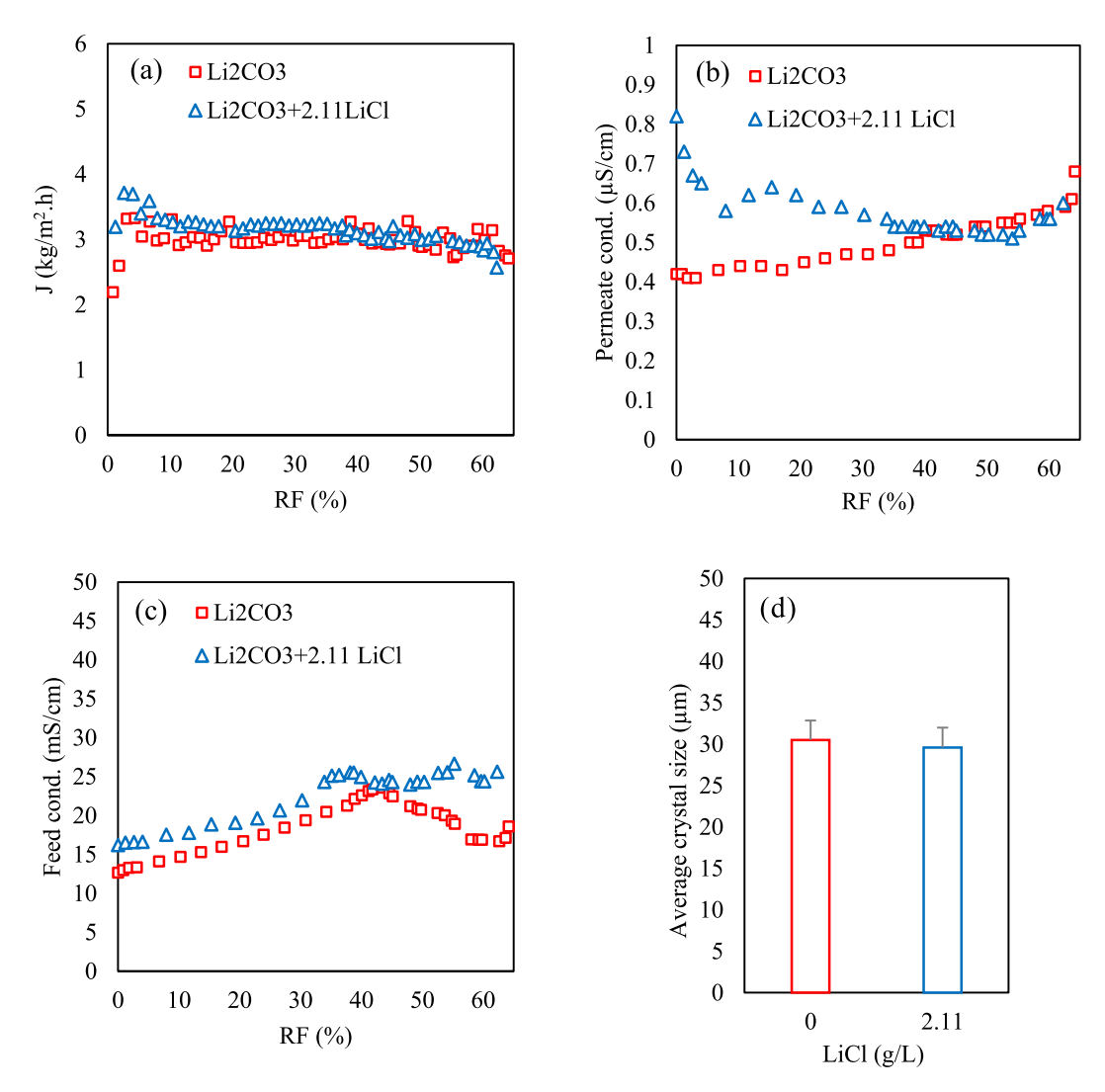


Fig. 8. (a) Permeate flux, (b) conductivity of permeate tank, (c) conductivity of feed tank, (d) average crystal size, (e) crystals elongation, (f) coefficient of variation, and (g) XRD patterns, for MCr experiments with LiCl (2.11 g/L) at constant feed temperature (60 ± 1 °C) and flowrate (1.3 L/min).

decreased. According to the observations, the $\rm Li_2CO_3$ crystals formed at a lower water recovery (i.e., 36.3 %) in comparison with the measured value for MCr experiment in the absence of inorganic salts at the same operating conditions (i.e., 41.7 % for the $\rm Li_2CO_3$ solution at 60 °C). This can be due to the reduced solubility of $\rm Li_2CO_3$ in the presence of LiCl. Unlike the salting-in effect of NaCl and KCl, this reduction in the solubility of lithium carbonate can be attributed to the common-ion effect (or salting-out), which can be explained as follows.

According to the common-ion effect, the solubility of a substance (Li_2CO_3 in this case) decreases if there is also a second electrolyte present that has an ion in common with the dominant species (LiCl in this case). Fig. S5-c shows the effect of LiCl presence in the solution on the solubility of the Li_2CO_3 . Any increase in the concentration of one or both components can lower the concentration of the counterion because the solubility product K_{sp} is a constant value (Eq. (S1)). As a result, the salt's apparent solubility is dwindling [69]. In particular, the presence of a common ion can cause the equilibrium to shift in a direction that reduces the concentration of the common ion. Consequently, the solubility of the electrolyte or sparingly soluble salt decreases, or in other words, its dissociation is suppressed [67]. That is why the Li_2CO_3 crystals could appear in a lower RF value in the presence of LiCl, while due to the reverse effect of other investigated salts and increasing in the Li_2CO_3 solubility, nucleation started at higher water recovery factors in the

presence of NaCl and KCl.

In spite of faster nucleation, the size of the Li_2CO_3 crystals did not change considerably. As could be observed in Fig. 8-d, the average crystal size remained almost constant for the Li_2CO_3 -LiCl solution, while in terms of other salt additives (i.e., Li_2CO_3 -NaCl and Li_2CO_3 -KCl), this parameter decreased (Figs. 5-d and 7-d). On the other hand, in terms of the elongation, slight decrease could be observed, and it decreased from 6.1 to 5.6 for the Li_2CO_3 and Li_2CO_3 -LiCl solutions, respectively (Fig. 8-e). Moreover, the CV of the obtained Li_2CO_3 crystals in the presence of LiCl remained in the range of 40, which is similar to the same value for crystals obtained from the Li_2CO_3 + KCl solution (Fig. 7-f). Furthermore, as could be expected, the obtained XRD patterns could confirm that the precipitated crystals were all Li_2CO_3 (Fig. 8-g).

3.2.4. Mixed salts presence

Further to the investigation of the effect of operating parameters (i. e., temperature and flowrate) and the presence of common salts on the crystallization of $\rm Li_2CO_3$ in binary and tertiary solutions, respectively, a more complex solution containing $\rm Li_2CO_3$ and combination of other salts (salts concentrations were 5.8, 0.5, and 2.11 g/L for NaCl, KCl, and LiCl, respectively) was introduced to the MCr system and the obtained results are presented in Fig. 9. Fig. 10 also shows the SEM image of the obtained crystals from this experiment, and the SEM image of a commercial

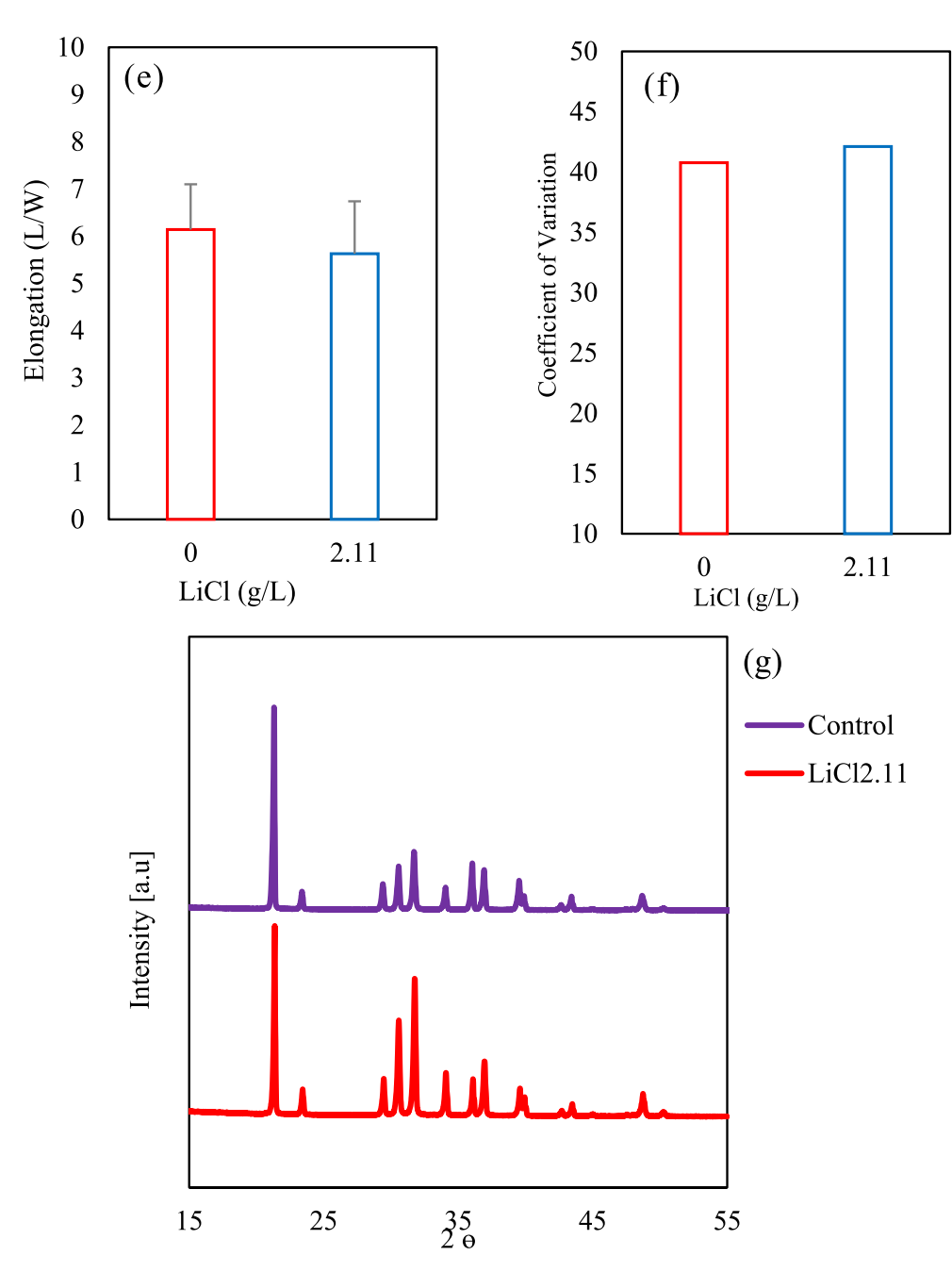


Fig. 8. (continued).

 $\rm Li_2CO_3$ sample. The MCr test was carried out at feed temperature of 60 $^{\circ}\text{C}$ and flowrate of 1.3 L/min.

According to the obtained results, the same trend for the permeate flux (i.e., the average permeate flux of $\sim\!\!3$ kg/m²-h) (Fig. 9-a) and the conductivity of the permeate tank (i.e., conductivity of permeate tank $<\!\!1$ µS/cm, after 9 h continuous test) (Fig. 9-b) was observed when the feed solution contains Li₂CO₃ and mixture of other salts (NaCl+KCl + LiCl). This confirms that the MCr process could properly process a more complex feed solution in presence of different salts. This argument is in good agreement with the literature indicating MCr can process brine and highly saline solutions in the absence of organic compounds and surfactant [27,74].

As could be expected, with using the mixed feed solution ($\text{Li}_2\text{CO}_3 + \text{NaCl+KCl} + \text{LiCl}$) the conductivity of the feed/crystallization tank increased (Fig. 9-c), and the very first crystals were observed at the water recovery factor of 37.8 %, which is lower than that of the

corresponding water recovery factor for the $\rm Li_2CO_3$ solution (41.7 %) under the same operating conditions. The slight change in the trend of the conductivity (blue triangles) of the feed solution indicates the start of crystallization (Fig. 9-c). Moreover, this water recovery factor is lower than that of the observed values for other feed solutions, $\rm Li_2CO_3$ -X (X: NaCl or KCl). Thus, it can be argued that, although the water recovery factor of the crystallization points slightly increased in comparison with the obtained value for the $\rm Li_2CO_3$ -LiCl solution, the common-ion effect still dominants the nucleation and crystal formation in the mixed salt solution.

In spite of starting the nucleation and crystallization at lower water recovery factor, the average crystal size decreased for the obtained crystals (Fig. 9-d). For example, in comparison with the obtained crystals from the Li₂CO₃ solution (30.5 μm), the obtained crystals from the mixed salts solution possess the average crystal size of 26.6 μm , which is smaller than the crystals from Li₂CO₃ + LiCl solutions, but larger than

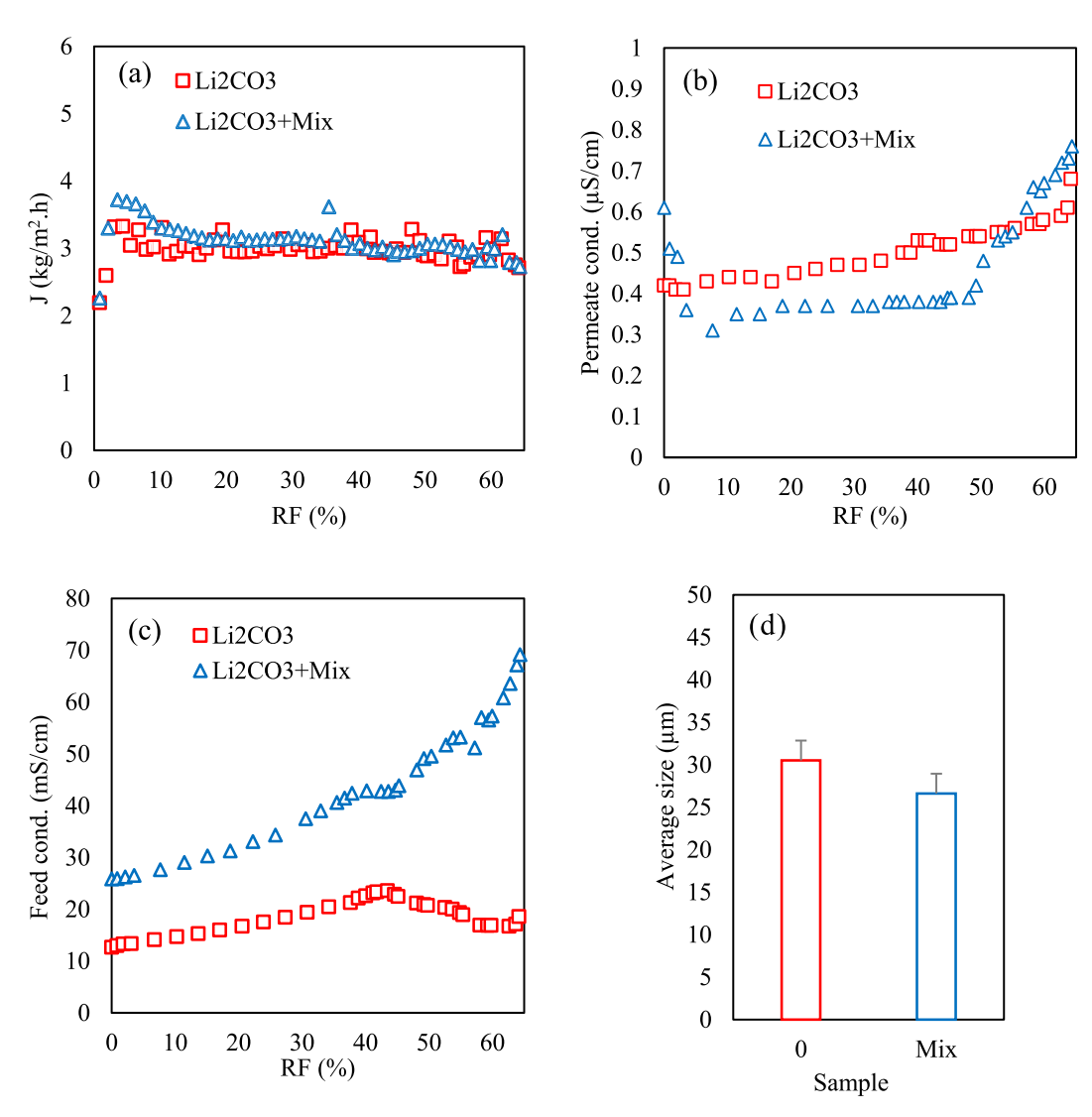


Fig. 9. (a) Permeate flux, (b) conductivity of permeate tank, (c) conductivity of feed tank, (d) average crystal size, (e) crystals elongation, (f) coefficient of variation, and (g) XRD pattern of obtained crystals, for MCr experiments of Li_2CO_3 solution in the presence of mixed salts $(\text{Li}_2\text{CO}_3\text{-NaCl-KCl-LiCl})$ at constant feed temperature $(60 \pm 1~^\circ\text{C})$ and flowrate (1.3~L/min). (h) Average permeates flux of the membrane module before and after the experiments at different temperatures $(40, 50, \text{ and } 60~^\circ\text{C})$ and constant flowrate (1.3~L/min).

the crystals from the Li₂CO₃-X (X: NaCl or KCl) solutions. The elongation and CV values of the obtained crystals, however, increased slightly (Fig. 9-e and -f). Moreover, the XRD pattern (Fig. 9-g) could confirm the purity of the obtained Li₂CO₃ crystals (Fig. 10-a), as no other inorganic salts precipitated, even in the presence of mixed salts in the feed solution. This is important as the correlation between the purity of the crystals and their sale price is evident. Based on the data obtained from Millipore-Sigma® (www.sigmaaldrich.com), it can be shown that the cost of the Li₂CO₃ crystals (Fig. 10-b) with purity levels of 99 %, 99.99 %, and 99.999 % are \$0.686, \$1.992, and \$3.386 per gram, respectively. Hence, the production of high purity crystals is necessary for the expansion of the MCr process on a commercial scale. In recent years, the researchers have also focused their efforts on the production of salts with excellent purity using the MCr, however, the most investigated salt was NaCl, which is often regarded as a cheaply accessible salt owing to its prevalence in brines [29]. Moreover, the future research can be focus on using MCr for direct Li₂CO₃ recovery from the complex brine solutions, in particular through a continuous operation and at higher RF values.

Furthermore, to consider the possibility of scaling on the membrane surface, the permeate flux of the membrane module was provided using

distilled water before and after the experiments. As could be observed in Fig. 9-h, there is no distinguishable difference between the permeate fluxes at each temperature. Thus, this shows that the considered cleaning procedure (first 1 h with cold water and then 1 h with hot water) could properly recover the membrane surface and that the scaling of the inorganic salts on the membrane surface was not the case in this work. However, further studies should be carried out to evaluate the membrane performance in terms of scaling and fouling when the system is run for higher water recovery factors (RF \geq 90 %).

4. Conclusions

In this research, the effect of operating conditions and presence of inorganic purities on the crystallization of Li_2CO_3 were investigated during the membrane crystallization (MCr) process. This can be promising for various Li end users, especially in the energy sector, due to the numerous advantages of the MCr process over the conventional options for recovery of high quality Li_2CO_3 . Moreover, highly pure water can also be produced simultaneously using this technology, which can be recovered as the makeup water source for further processing of Li_2CO_3

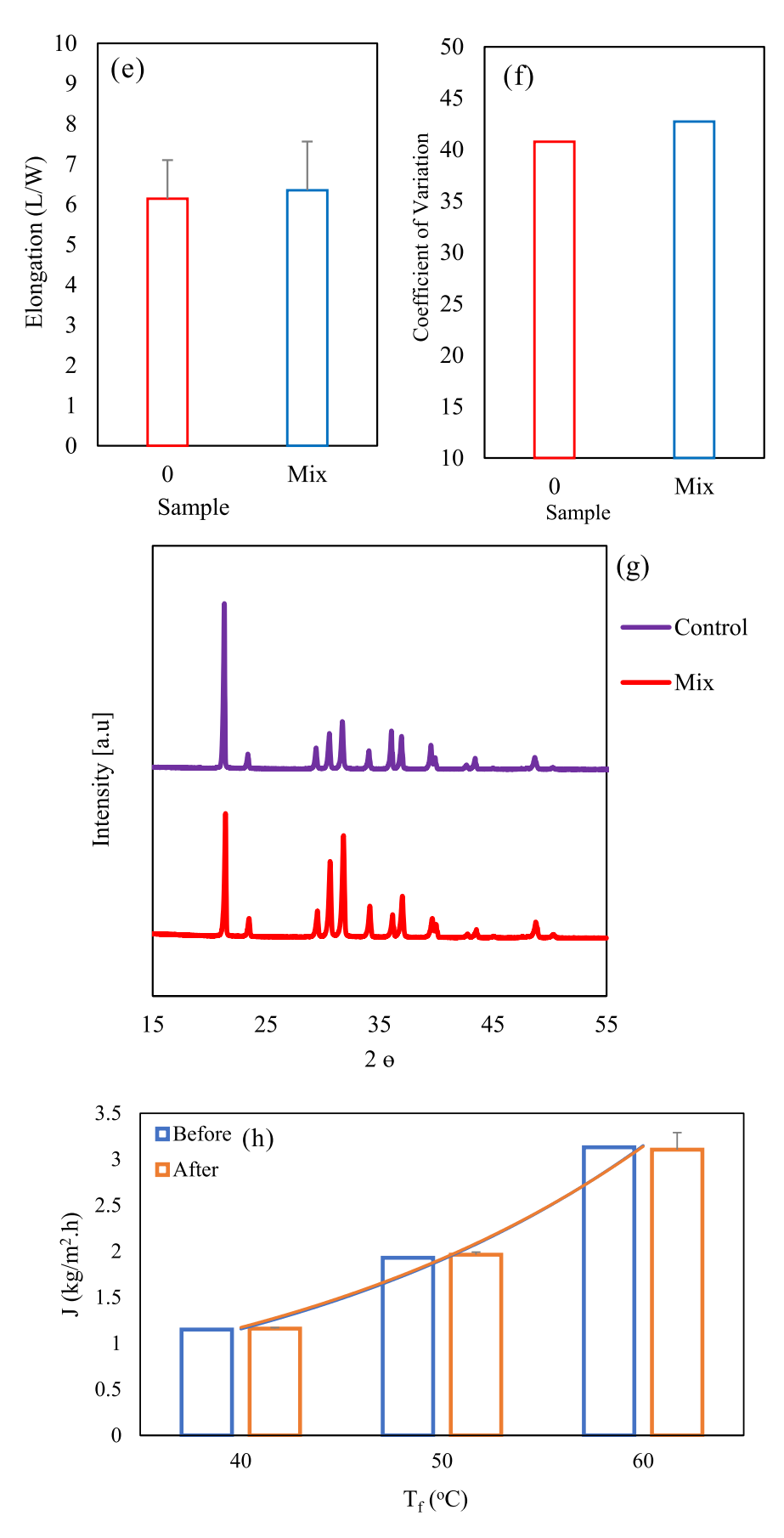
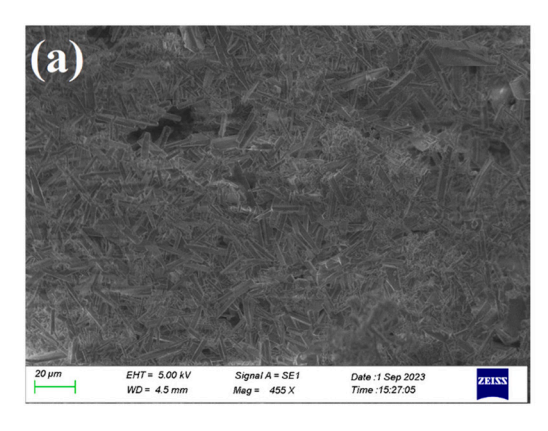


Fig. 9. (continued).



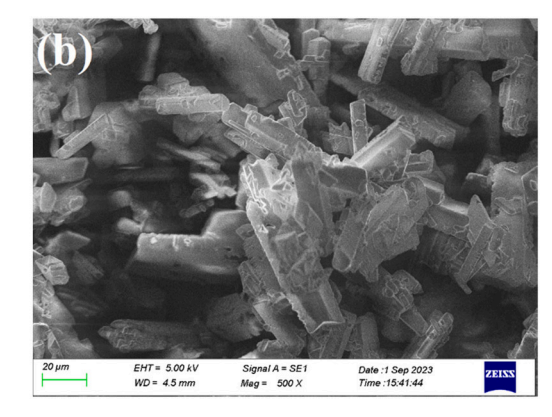


Fig. 10. SEM images of Li₂CO₃ crystals (a) obtained from the solution with mixed salts and (b) commercial Li₂CO₃ crystals.

crystals.

The obtained results revealed that feed temperature dominates the $\rm Li_2CO_3$ crystal formation and characteristics, such as average size. Moreover, the higher the feed temperature, the higher the permeate flux. The presence of inorganic salts can also affect the MCr performance in terms of crystal formation. NaCl and KCl delayed the formation of crystals, mainly due to their effect on increasing the solubility of $\rm Li_2CO_3$ and salting-in effect. However, the presence of salts with the commonion effect, such as LiCl, could contribute to faster crystallization. This can be important for the future research in terms of combination of MCr with other technologies for recovery of $\rm Li_2CO_3$ from brine streams.

Furthermore, there are some issues which should be addressed in the future works, such as continuous MCr process at high water recovery values, selective Li recovery from a multicomponent brine, energy conservation, and utilizing renewable energy sources for a sustainable and efficient Li recovery using the MCr process. Future studies can also be focused on integration of conventional technologies with MCr, either as a pre-treatment or post-treatment, and their performance for lithium recovery. Overall, it can be concluded that the MCr process can be a game changer for direct and continuous production of high quality Li₂CO₃ crystals from brines.

CRediT authorship contribution statement

Mohammad Mahdi A. Shirazi: Methodology, Investigation, Validation, Visualization, Writing – original draft. **Aamer Ali:** Conceptualization, Methodology, Writing – review & editing, Supervision. **Cejna Anna Quist-Jensen:** Conceptualization, Methodology, Writing – review & editing, Supervision, Funding acquisition.

Declaration of competing interest

The authors declare that they have no known competing financial interests or personal relationships that could have appeared to influence the work reported in this paper.

Data availability

Data will be made available on request.

Acknowledgement

The authors are greatly thankful to the Poul Due Jensen Foundation for funding this work through the project "Membrane Distillation and Membrane Crystallization for recovery of water and minerals from waste streams". Moreover, the help provided by Mr. Bastian Stiem Kirkebæk is also highly appreciated.

Appendix A. Supplementary data

Supplementary data to this article can be found online at https://doi.org/10.1016/j.desal.2023.117109.

References

- [1] A. Ali, C.A. Quist-Jensen, M.K. Jørgensen, A. Siekierka, M.L. Christensen, M. Bryjak, C. Hélix-Nielsen, E. Drioli, A review of membrane crystallization, forward osmosis and membrane capacitive deionization for liquid mining, Resour. Conserv. Recycl. 168 (2021), 105273, https://doi.org/10.1016/J. RESCONREC.2020.105273.
- [2] A. Ali, C. Quist-Jensen, F. Macedonio, E. Drioli, Application of membrane crystallization for minerals' recovery from produced water, Membranes (Basel) 5 (2015) 772–792, https://doi.org/10.3390/membranes5040772.
- [3] A. Panagopoulos, Techno-economic assessment of zero liquid discharge (ZLD) systems for sustainable treatment, minimization and valorization of seawater brine, J. Environ. Manag. 306 (2022), 114488, https://doi.org/10.1016/J. JENVMAN.2022.114488.
- [4] A. Panagopoulos, Brine management (saline water & wastewater effluents): sustainable utilization and resource recovery strategy through minimal and zero liquid discharge (MLD & ZLD) desalination systems, Chem. Eng. Process. Process Intensif. 176 (2022), 108944, https://doi.org/10.1016/J.CEP.2022.108944.
- [5] A. Khalil, S. Mohammed, R. Hashaikeh, N. Hilal, Lithium recovery from brine: recent developments and challenges, Desalination 528 (2022), 115611, https://doi.org/10.1016/J.DESAL.2022.115611.
- [6] F. Meng, J. McNeice, S.S. Zadeh, A. Ghahreman, Review of lithium production and recovery from minerals, brines, and lithium-ion batteries, Miner. Process. Extr. Metall. Rev. 42 (2021) 123–141, https://doi.org/10.1080/ 08827508.2019.1668387
- [7] W.T. Stringfellow, P.F. Dobson, Technology for the recovery of lithium from geothermal brines, Energies (Basel) 14 (2021) 6805, https://doi.org/10.3390/ en14206805.
- [8] H. Ambrose, A. Kendall, Understanding the future of lithium: part 1, resource model, J. Ind. Ecol. 24 (2020) 80–89, https://doi.org/10.1111/jiec.12949.
- [9] J. Rioyo, S. Tuset, R. Grau, Lithium extraction from Spodumene by the traditional sulfuric acid process: a review, Miner. Process. Extr. Metall. Rev. 43 (2022) 97–106, https://doi.org/10.1080/08827508.2020.1798234.
- [10] G. Battaglia, L. Berkemeyer, A. Cipollina, J.L. Cortina, M. Fernandez de Labastida, J. Lopez Rodriguez, D. Winter, Recovery of lithium carbonate from dilute Li-rich brine via homogenous and heterogeneous precipitation, Ind. Eng. Chem. Res. 61 (2022) 13589–13602, https://doi.org/10.1021/acs.iecr.2c01397.
- [11] Y. Zhang, Y. Hu, L. Wang, W. Sun, Systematic review of lithium extraction from salt-lake brines via precipitation approaches, Miner. Eng. 139 (2019), 105868, https://doi.org/10.1016/j.mineng.2019.105868.
- [12] H. Bae, Y. Kim, Technologies of lithium recycling from waste lithium ion batteries: a review, Mater. Adv. 2 (2021) 3234–3250, https://doi.org/10.1039/ DIMAGGAGE
- [13] L. Wu, C. Zhang, S. Kim, T.A. Hatton, H. Mo, T.D. Waite, Lithium recovery using electrochemical technologies: advances and challenges, Water Res. 221 (2022), 118822, https://doi.org/10.1016/J.WATRES.2022.118822.
- [14] X. Zhang, W. Zhao, Y. Zhang, V. Jegatheesan, A review of resource recovery from seawater desalination brine, Rev. Environ. Sci. Biotechnol. 20 (2021) 333–361, https://doi.org/10.1007/s11157-021-09570-4.
- [15] Y. Orooji, Z. Nezafat, M. Nasrollahzadeh, N. Shafiei, M. Afsari, K. Pakzad, A. Razmjou, Recent advances in nanomaterial development for lithium ion-sieving technologies, Desalination 529 (2022), 115624, https://doi.org/10.1016/J. DFSAL.2022.115624.
- [16] X. Li, Y. Mo, W. Qing, S. Shao, C.Y. Tang, J. Li, Membrane-based technologies for lithium recovery from water lithium resources: a review, J. Membr. Sci. 591 (2019), 117317, https://doi.org/10.1016/J.MEMSCI.2019.117317.

- [17] S. Xu, J. Song, Q. Bi, Q. Chen, W.-M. Zhang, Z. Qian, L. Zhang, S. Xu, N. Tang, T. He, Extraction of lithium from Chinese salt-lake brines by membranes: design and practice, J. Membr. Sci. 635 (2021), 119441, https://doi.org/10.1016/j. memsci 2021 119441
- [18] J. Hou, H. Zhang, A.W. Thornton, A.J. Hill, H. Wang, K. Konstas, Lithium extraction by emerging metal–organic framework-based membranes, Adv. Funct. Mater. 31 (2021), https://doi.org/10.1002/adfm.202105991.
- [19] T. Zhang, W. Zheng, Q. Wang, Z. Wu, Z. Wang, Designed strategies of nanofiltration technology for Mg2+/Li+ separation from salt-lake brine: a comprehensive review, Desalination 546 (2023), 116205, https://doi.org/ 10.1016/J.DESAL.2022.116205.
- [20] J. Li, M. Wang, Y. Zhao, H. Yang, Y. Zhong, Enrichment of lithium from salt lake brine by forward osmosis, R. Soc. Open Sci. 5 (2018), 180965, https://doi.org/ 10.1098/rsos.180965.
- [21] P.C.B.W. Mustika, W. Astuti, S. Sumardi, H.T.B.M. Petrus, Sutijan, Separation characteristic and selectivity of lithium from geothermal brine using forward osmosis, J. Sustain. Metall. 8 (2022) 1769–1784, https://doi.org/10.1007/s40831-022.00602.
- [22] H. Yu, G. Naidu, C. Zhang, C. Wang, A. Razmjou, D.S. Han, T. He, H. Shon, Metal-based adsorbents for lithium recovery from aqueous resources, Desalination 539 (2022), 115951, https://doi.org/10.1016/J.DESAL.2022.115951.
- [23] S. Raggam, M. Mohammad, Y. Choo, G. Danasamy, M. Zargar, H. Kyong Shon, A. Razmjou, Advances in metal organic framework (MOF) – based membranes and adsorbents for lithium-ion extraction, Sep. Purif. Technol. 307 (2023), 122628, https://doi.org/10.1016/J.SEPPUR.2022.122628.
- [24] C. Quist-Jensen, F. Macedonio, E. Drioli, Integrated membrane desalination systems with membrane crystallization units for resource recovery: a new approach for mining from the sea, Crystals (Basel) 6 (2016) 36, https://doi.org/10.3390/ cryst6040036.
- [25] C.A. Quist-Jensen, A. Ali, E. Drioli, F. Macedonio, Perspectives on mining from sea and other alternative strategies for minerals and water recovery – the development of novel membrane operations, J. Taiwan Inst. Chem. Eng. 94 (2019) 129–134, https://doi.org/10.1016/J.JTICE.2018.02.002.
- [26] M.C. Sparenberg, S. Chergaoui, V. Sang Sefidi, P. Luis, Crystallization control via membrane distillation-crystallization: a review, Desalination 519 (2021), 115315, https://doi.org/10.1016/J.DESAL.2021.115315.
- [27] M.C. Sparenberg, S. Chergaoui, V. Sang Sefidi, P. Luis, Crystallization control via membrane distillation-crystallization: a review, Desalination 519 (2021), 115315, https://doi.org/10.1016/J.DESAL.2021.115315.
- [28] A. Yadav, P.K. Labhasetwar, V.K. Shahi, Membrane distillation crystallization technology for zero liquid discharge and resource recovery: opportunities, challenges and futuristic perspectives, Sci. Total Environ. 806 (2022), 150692, https://doi.org/10.1016/J.SCITOTENV.2021.150692.
- [29] X. Zhang, R. Koirala, B. Pramanik, L. Fan, A. Date, V. Jegatheesan, Challenges and advancements in membrane distillation crystallization for industrial applications, Environ. Res. 234 (2023), 116577, https://doi.org/10.1016/j. envres.2023.116577.
- [30] C.A. Quist-Jensen, J.M. Sørensen, A. Svenstrup, L. Scarpa, T.S. Carlsen, H. C. Jensen, L. Wybrandt, M.L. Christensen, Membrane crystallization for phosphorus recovery and ammonia stripping from reject water from sludge dewatering process, Desalination 440 (2018) 156–160, https://doi.org/10.1016/J. DESAL.2017.11.034.
- [31] C.A. Quist-Jensen, F. Macedonio, D. Horbez, E. Drioli, Reclamation of sodium sulfate from industrial wastewater by using membrane distillation and membrane crystallization, Desalination 401 (2017) 112–119, https://doi.org/10.1016/J. DFSAI_2016.05.007.
- [32] I.R. Salmón, K. Simon, C. Clérin, P. Luis, Salt recovery from wastewater using membrane distillation–crystallization, Cryst. Growth Des. 18 (2018) 7275–7285, https://doi.org/10.1021/acs.cgd.8b00580.
- [33] B. Tang, G. Yu, J. Fang, T. Shi, Recovery of high-purity silver directly from dilute effluents by an emulsion liquid membrane-crystallization process, J. Hazard. Mater. 177 (2010) 377–383, https://doi.org/10.1016/J.JHAZMAT.2009.12.042.
- [34] G. Ji, W. Wang, H. Chen, S. Yang, J. Sun, W. Fu, B. Yang, Z. Huang, Sustainable potassium chloride production from concentrated KCl brine via a membrane-promoted crystallization process, Desalination 521 (2022), 115389, https://doi.org/10.1016/J.DESAL.2021.115389.
- [35] M.C. Sparenberg, I. Ruiz Salmón, P. Luis, Economic evaluation of salt recovery from wastewater via membrane distillation-crystallization, Sep. Purif. Technol. 235 (2020), 116075, https://doi.org/10.1016/J.SEPPUR.2019.116075.
- [36] P. Das, S. Dutta, K.K. Singh, Insights into membrane crystallization: a sustainable tool for value added product recovery from effluent streams, Sep. Purif. Technol. 257 (2021), 117666, https://doi.org/10.1016/J.SEPPUR.2020.117666.
- [37] C.A. Quist-Jensen, A. Ali, S. Mondal, F. Macedonio, E. Drioli, A study of membrane distillation and crystallization for lithium recovery from high-concentrated aqueous solutions, J. Membr. Sci. 505 (2016) 167–173, https://doi.org/10.1016/J. MEMSCI 2016, 01 033
- [38] A. Cerda, M. Quilaqueo, L. Barros, G. Seriche, M. Gim-Krumm, S. Santoro, A. H. Avci, J. Romero, E. Curcio, H. Estay, Recovering water from lithium-rich brines by a fractionation process based on membrane distillation-crystallization, J. Water Process Eng. 41 (2021), 102063, https://doi.org/10.1016/j.jwpe.2021.102063.
- [39] M. Quilaqueo, G. Seriche, L. Barros, C. González, J. Romero, R. Ruby-Figueroa, S. Santoro, E. Curcio, H. Estay, Water recovery assessment from hypersaline lithium-rich brines using membrane distillation-crystallization, Desalination 537 (2022), 115887, https://doi.org/10.1016/j.desal.2022.115887.

- [40] M. Qasim, I.U. Samad, N.A. Darwish, N. Hilal, Comprehensive review of membrane design and synthesis for membrane distillation, Desalination 518 (2021), 115168, https://doi.org/10.1016/j.desal.2021.115168.
- [41] F.E. Ahmed, B.S. Lalia, R. Hashaikeh, N. Hilal, Alternative heating techniques in membrane distillation: a review, Desalination 496 (2020), 114713, https://doi. org/10.1016/J.DESAL.2020.114713.
- [42] W.N.A. Wan Osman, N.I. Mat Nawi, S. Samsuri, M.R. Bilad, Y. Wibisono, E. Hernández Yáñez, J. Md Saad, A review on recent progress in membrane distillation crystallization, ChemBioEng Rev. 9 (2022) 93–109, https://doi.org/ 10.1002/cben.202100034.
- [43] G. Battaglia, L. Berkemeyer, A. Cipollina, J.L. Cortina, M. Fernandez de Labastida, J. Lopez Rodriguez, D. Winter, Recovery of lithium carbonate from dilute Li-rich brine via homogenous and heterogeneous precipitation, Ind. Eng. Chem. Res. 61 (2022) 13589–13602, https://doi.org/10.1021/acs.iecr.2c01397.
- [44] M. Figueira, D. Rodríguez-Jiménez, J. López, M. Reig, J.L. Cortina, C. Valderrama, Experimental and economic evaluation of nanofiltration as a pre-treatment for added-value elements recovery from seawater desalination brines, Desalination 549 (2023), 116321, https://doi.org/10.1016/j.desal.2022.116321.
- [45] Y. Huang, C. Xiao, Q. Huang, H. Liu, J. Zhao, Progress on polymeric hollow fiber membrane preparation technique from the perspective of green and sustainable development, Chem. Eng. J. 403 (2021), 126295, https://doi.org/10.1016/j. cej.2020.126295.
- [46] A.S. Niknejad, S. Bazgir, A. Sadeghzadeh, M.M.A. Shirazi, Styrene-acrylonitrile (SAN) nanofibrous membranes with unique properties for desalination by direct contact membrane distillation (DCMD) process, Desalination 488 (2020), 114502, https://doi.org/10.1016/j.desal.2020.114502.
- [47] C.A. Quist-Jensen, J.M. Sørensen, A. Svenstrup, L. Scarpa, T.S. Carlsen, H. C. Jensen, L. Wybrandt, M.L. Christensen, Membrane crystallization for phosphorus recovery and ammonia stripping from reject water from sludge dewatering process, Desalination 440 (2018) 156–160, https://doi.org/10.1016/J. DESAL.2017.11.034.
- [48] A. Ali, C.A. Quist-Jensen, E. Drioli, F. Macedonio, Evaluation of integrated microfiltration and membrane distillation/crystallization processes for produced water treatment, Desalination 434 (2018) 161–168, https://doi.org/10.1016/J. DESAL.2017.11.035.
- [49] M. Khayet, Membranes and theoretical modeling of membrane distillation: a review, Adv. Colloid Interf. Sci. 164 (2011) 56–88, https://doi.org/10.1016/j. cis.2010.09.005.
- [50] A. Alkhudhiri, N. Darwish, N. Hilal, Membrane distillation: a comprehensive review, Desalination 287 (2012) 2–18, https://doi.org/10.1016/j. desal.2011.08.027.
- [51] M.M.A. Shirazi, A. Kargari, A.F. Ismail, T. Matsuura, Computational fluid dynamic (CFD) opportunities applied to the membrane distillation process: state-of-the-art and perspectives, Desalination 377 (2016) 73–90, https://doi.org/10.1016/j. desal.2015.09.010.
- [52] I. Hitsov, T. Maere, K. de Sitter, C. Dotremont, I. Nopens, Modelling approaches in membrane distillation: a critical review, Sep. Purif. Technol. 142 (2015) 48–64, https://doi.org/10.1016/J.SEPPUR.2014.12.026.
- [53] Z. Kuang, R. Long, Z. Liu, W. Liu, Analysis of temperature and concentration polarizations for performance improvement in direct contact membrane distillation, Int. J. Heat Mass Transf. 145 (2019), 118724, https://doi.org/ 10.1016/j.ijheatmasstransfer.2019.118724.
- [54] I. Ruiz Salmón, P. Luis, Membrane crystallization via membrane distillation, chemical engineering and processing, Process Intens. 123 (2018) 258–271, https://doi.org/10.1016/j.cep.2017.11.017.
- [55] W. Cheng, Z. Li, F. Cheng, Solubility of Li2CO3 in Na-K-Li-Cl brines from 20 to 90 °C, J. Chem. Thermodyn. 67 (2013) 74–82, https://doi.org/10.1016/J. https://doi.org/10.1016/J.
- [56] S. Shankar Naik, S.J. Lee, Y. Yu, A.M. Al-Mohaimeed, J. Theerthagiri, M.Y. Choi, Novel approach for the synthesis and recovery of lithium carbonate using a pulsed laser irradiation technique, Mater. Lett. 308 (2022), 131218, https://doi.org/ 10.1016/j.mailet.2021.131218.
- [57] Y. Yun, R. Ma, W. Zhang, A.G. Fane, J. Li, Direct contact membrane distillation mechanism for high concentration NaCl solutions, Desalination 188 (2006) 251–262, https://doi.org/10.1016/J.DESAL.2005.04.123.
- [58] H.J. Hwang, K. He, S. Gray, J. Zhang, I.S. Moon, Direct contact membrane distillation (DCMD): experimental study on the commercial PTFE membrane and modeling, J. Membr. Sci. 371 (2011) 90–98, https://doi.org/10.1016/J. MEMSCI.2011.01.020.
- [59] Y. Choi, G. Naidu, L.D. Nghiem, S. Lee, S. Vigneswaran, Membrane distillation crystallization for brine mining and zero liquid discharge: opportunities, challenges, and recent progress, Environ. Sci. (Camb.) 5 (2019) 1202–1221, https://doi.org/10.1039/C9EW00157C.
- [60] J. Kim, J. Kim, S. Hong, Recovery of water and minerals from shale gas produced water by membrane distillation crystallization, Water Res. 129 (2018) 447–459, https://doi.org/10.1016/j.watres.2017.11.017.
- [61] G. Chen, Y. Lu, W.B. Krantz, R. Wang, A.G. Fane, Optimization of operating conditions for a continuous membrane distillation crystallization process with zero salty water discharge, J. Membr. Sci. 450 (2014) 1–11, https://doi.org/10.1016/j. memsci.2013.08.034.
- [62] K.J. Lu, Z.L. Cheng, J. Chang, L. Luo, T.-S. Chung, Design of zero liquid discharge desalination (ZLDD) systems consisting of freeze desalination, membrane distillation, and crystallization powered by green energies, Desalination 458 (2019) 66–75, https://doi.org/10.1016/j.desal.2019.02.001.

- [63] A. Ali, C. Quist-Jensen, F. Macedonio, E. Drioli, Application of membrane crystallization for minerals' recovery from produced water, Membranes (Basel) 5 (2015) 772–792, https://doi.org/10.3390/membranes5040772.
- [64] H. Chamani, J. Woloszyn, T. Matsuura, D. Rana, C.Q. Lan, Pore wetting in membrane distillation: a comprehensive review, Prog. Mater. Sci. 122 (2021), 100843, https://doi.org/10.1016/j.pmatsci.2021.100843.
- [65] M. Rezaei, D.M. Warsinger, J.H. Lienhard V, M.C. Duke, T. Matsuura, W. M. Samhaber, Wetting phenomena in membrane distillation: mechanisms, reversal, and prevention, Water Res. 139 (2018) 329–352, https://doi.org/10.1016/j.watres.2018.03.058.
- [66] H. Langer, H. Offermann, On the solubility of sodium chloride in water, J. Cryst. Growth 60 (1982) 389–392, https://doi.org/10.1016/0022-0248(82)90116-6.
- [67] V.L. Snoeyink, D. Jenkins, Water Chemistry, John Wiley & Sons, New York, 1980.
- [68] B.O. Myrvold, Salting-out and Salting-in Experiments With Lignosulfonates (LSs) 67, Hfsg, 2013, pp. 549–557, https://doi.org/10.1515/hf-2012-0163.
- [69] W. Beckmann, Crystallization, Wiley-VCH Verlag GmbH & Co. KGaA, 2013.

- [70] H. Wang, B. Du, M. Wang, Study of the solubility, supersolubility and metastable zone width of Li ₂ CO ₃ in the LiCl–NaCl–KCl–Na ₂ SO ₄ system from 293.15 to 353.15K, J. Chem. Eng. Data 63 (2018) 1429–1434, https://doi.org/10.1021/acs. iced 7b01012
- [71] C.-C. Ko, A. Ali, E. Drioli, K.-L. Tung, C.-H. Chen, Y.-R. Chen, F. Macedonio, Performance of ceramic membrane in vacuum membrane distillation and in vacuum membrane crystallization, Desalination 440 (2018) 48–58, https://doi. org/10.1016/j.desal.2018.03.011.
- [72] R. Zangi, Can salting-in/salting-out ions be classified as chaotropes/kosmotropes? J. Phys. Chem. B 114 (2010) 643–650, https://doi.org/10.1021/jp909034c.
- [73] A. Seidell, Solubilities of Inorganic and Organic Substances; A Handbook Of The Most Reliable Quantitative Solubility Determinations, Alpha edition, 2020.
- [74] X. Jiang, L. Tuo, D. Lu, B. Hou, W. Chen, G. He, Progress in membrane distillation crystallization: process models, crystallization control and innovative applications, Front. Chem. Sci. Eng. 11 (2017) 647–662, https://doi.org/10.1007/s11705-017-1649-8.